HIGH-PERFORMANCE HEAT PIPES FOR

HEAT RECOVERY APPLICATIONS

Contract No. NAS5-25357

FINAL REPORT

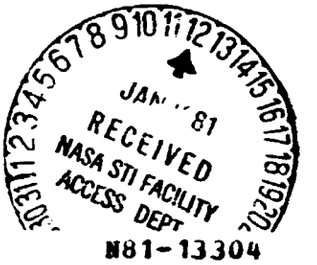

Prepared
For

Goddard Space Flight Center
National Aeronautics and Space Administration
Greenbelt, Maryland

September 1979

SIGMA RESEARCH, INC.
2950 GEORGE WASHINGTON WAY
RICHLAND, WASHINGTON 99352
(509) 375-0682

This document is the final report submitted by Sigma Research, Inc., Richland, Washington, under Contract No. NAS5-25357. R. McIntosh was the NASA Technical Manager.

HIGH-PERFORMANCE HEAT PIPES FOR HEAT RECOVERY APPLICATIONS

E. W. Saaski
J. H. Hartl

SIGMA RESEARCH, INC.
2950 George Washington Way
Richland, Washington 99352

September 1979

Work performed under Contract No. NAS5-25357

CONTENTS

ABSTRACT

Methods to improve the performance of reflux heat pipes for heat recovery applications have been examined both analytically and experimentally. A survey of literature models for the estimation of reflux heat pipe transport capacity was performed and these various models were compared with experimental data. A high transport capacity reflux heat pipe was developed that provides up to a factor of 10 capacity improvement over conventional open-tube designs; analytical models were developed for this device and incorporated into a computer program "HPIPE". Good agreement of the model predictions with data for R-11 and benzene reflux heat pipes was obtained.

1.0 INTRODUCTION

This report discusses analyses and experiments directed towards the development of an improved reflux heat pipe for heat recovery applications. The result of this work has been a "cocurrent flow" heat pipe that has a transport capacity of about 10 times that of a conventional open-core heat pipe or two-phase thermosyphon. This performance increase is the result of introducing a relatively simple plate/tube separator assembly into the heat pipe vapor core. This separator system provides cocurrent vapor-liquid flow in all heat pipe sections and eliminates the vapor/liquid countercurrent shear that commonly limits reflux heat pipe capacity and causes vibration and thermal instability.

Section 2 of this report discusses and compares various literature models of reflux heat pipe transport capacity and describes the analytical models developed for cocurrent flow heat pipes. The thermal requirements of heat pipes for heat recovery applications are outlined and compared to the various heat pipe capacities predicted for conventional and cocurrent flow heat pipes.

Section 3 presents a discussion of experimental tests performed in support of the analytical studies and a comparison of these tests with model predictions. Section 4 is a summary of the work performed and a discussion of further areas meriting study.

2.0 ANALYSIS

This section describes past and present art in the field of reflux heat pipes and discusses the transport requirements of reflux heat pipes used for heat recovery applications. Expressions proposed by various investigators for estimation of reflux heat pipe transport capacity are presented and compared with experimental data. A new reflux heat pipe design is discussed that has a particularly high transport capacity and an analytical model for the device is presented.

2.1 Reflux Heat Pipes

2.1.1 Prior Art

The application of reflux heat pipes or two-phase thermosyphons to energy-related problems in a sense began prior to the development of heat pipes in that the concept of using closed heat transfer tubes partially filled with a vaporizable fluid was the subject of U. S. patent activity as early as the 1920's. Figure 2.1.1 shows the "Heat Transfer Means" presented by F. W. Gay in 1929 for recuperator heat recovery.[1] The air inlet and stock exhaust ducts were coupled by

> "sealed tubes containing a volatile liquid, said tubes having their lower ends in contact with the outgoing hot stack gases and their upper ends in contact with ingoing air, so that said volatile liquid boils in the lower ends of the tubes under the influence of the heat of the stack gases to produce a hot vapor which rises to the upper ends of the tubes, the heat thus carried to the upper tube ends being radiated therefrom to the air, and such transfer of heat operating to cool and condense said vapor for return to the lower tube ends, so that the cycle of heat transfer operations thus produced is continuously repeated."

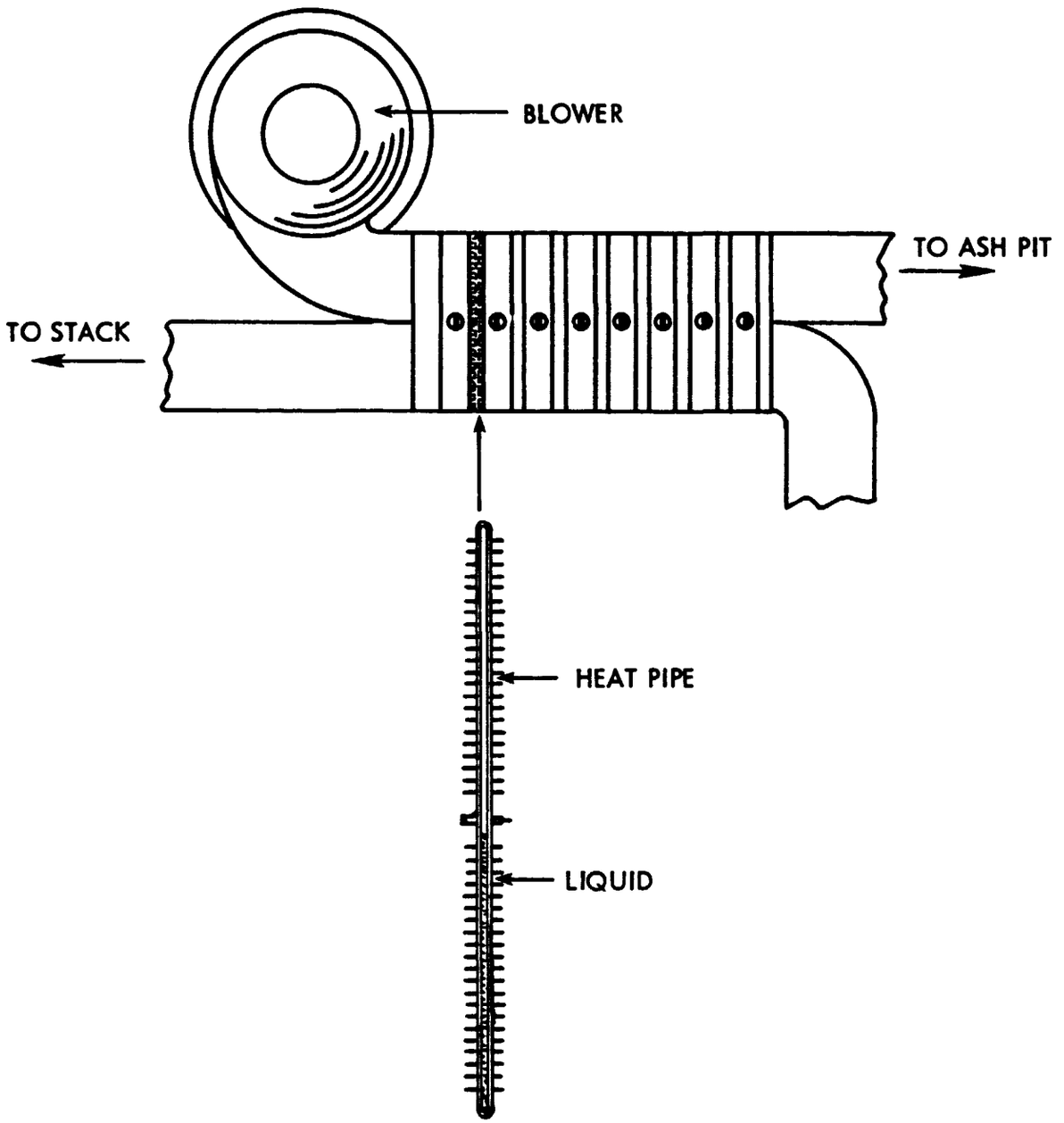

FIGURE 2.1.1. REFLUX HEAT PIPE OR TWO-PHASE THERMOSYPHON PROPOSED FOR HEAT RECOVERY APPLICATIONS IN 1929.

In a second patent issued in 1930,[2] Gay applied these reflux tubes to the cooling of underground electric transmission lines.

In 1965, E. L. Long patented a refluxing two-phase heat transfer tube[3] used for permafrost stabilization which was essentially identical to the heat transfer tube of Gay in 1929, while in 1973, E. D. Waters patented the Cryoanchor®,[4] a second permafrost stabilization device relying on a refluxing two-phase liquid/vapor cycle. Other permafrost-type reflux devices are referenced by O'Byrne.[5]

The first mention of capillary wick pumping as a means of liquid distribution in a two-phase heat transfer tube was in a 1938 patent[6] and the 1944 patent of Gaugler,[6a] and during the 1960's and early 1970's, it was customary to identify two-phase heat transfer tubes without a capillary wick and with substantial fluid charges as "two-phase thermosyphons" while those relying on capillary action and thin-film evaporation and condensation were called "heat pipes".[7] This distinction has gradually been lost, and numerous references can now be found to devices which would have once been called thermosyphons that are now called heat pipes. Many of these reflux tubes are substantially overloaded but employ wicking or grooves for capillary liquid transfer, and hence the distinction is also being lost from an operational standpoint. In this report, all these heat transfer devices will be termed "heat pipes".

R. A. Ares obtained a patent in 1972 on an air-to-air heat pipe heat recovery system similar to Gay's that was for the precooling of air for large refrigerated vaults and produce ripening rooms.[8] The duct-to-duct heat pipes were used in combination with a vapor compression cycle refrigeration unit to ostensibly reduce the refrigeration load required for make-up air. In 1973, J. E. Runyan and G. M. Grover of Q-Dot Corporation patented a circumferentially grooved heat pipe for near-horizontal disposition in air-to-air heat recovery heat exchangers[9] which used a cross-shaped extrusion to separate the vapor and liquid and thereby reduce wave action, slugging, and other transport-reducing liquid-vapor interactions (Figure 2.1.2). This was followed in 1974 by a

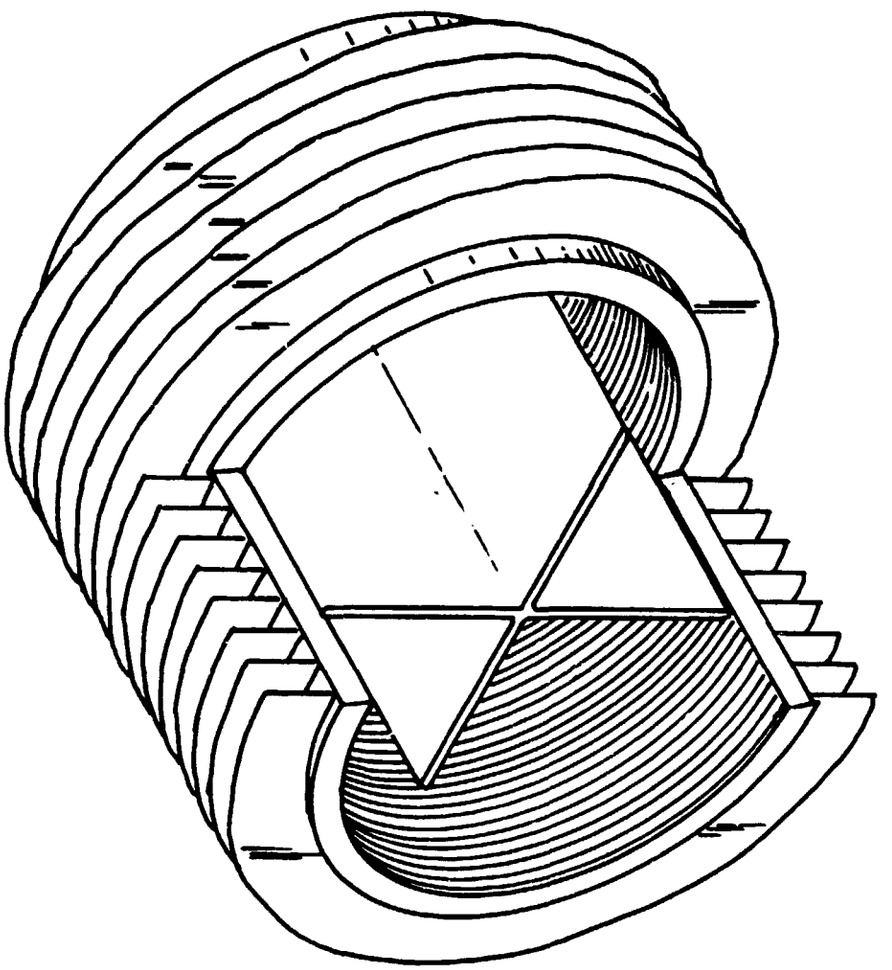

FIGURE 2.1.2. REFLUX HEAT PIPE SEPARATOR PROPOSED BY Runyan AND GROVER.

second air-to-air heat pipe heat exchanger patent by H. G. Barkmann of Q-Dot Corporation,[10] in which the heat pipes were again very nearly horizontal, and could be regulated in transport capacity by tipping. This patent also covered heat pipes with no internal wick or grooving, and was a continuation of a patent originally abandoned in 1969. Both of these patents indicated a nominal liquid load of about one-third the total heat pipe volume.

In 1975, R. L. Pessolano et al received a patent on an air-to-air or fluid-to-air heat pipe heat exchanger for domestic or industrial heating systems that is very similar to Gay's except that the heat pipes are specified to contain a capillary material for liquid transport and to not be ".....dependent on gravity for operation."[11]

M. A. Ruch and G. M. Grover of Q-Dot Corporation presented a paper at the 1976 International Heat Pipe Conference describing heat pipe thermal recovery applications and design features of heat pipe heat exchangers.[12] The heat pipes described as manufactured by their company were not like those described in the patents (9) and (10), but rather were characterized as filled with liquid to 50 to 70% of free volume and as having a small-diameter tube 60 to 80% of the overall length within the larger diameter tube to transport liquid back to the evaporator section. Transport capacities with halogenated hydrocarbon fluids at 2 to 10 atmospheres were stated to be in the range of 1500 to 2500 watts for a 2.3 cm I.D. tube, and three to four times greater with the return artery. A patent was awarded in 1977 to Grover [34] as a result of this work.

In summary, heat pipes or heat pipe-like two-phase heat transfer tubes have been used or proposed in the United States for heat recovery applications since 1929 or earlier, but have only received substantial commercial attention over the past ten years. Improvements to the basic heat pipe for reflux operation have been relatively few, with the use of capillary wick or grooves as a liquid transport means being one of the most significant advancements over the past 40 years. Some preliminary work has been done on improving transport capacity, but as will be discussed in the following section, most analytical and experimental work is still centered around modeling of the basic reflux tube as described by Gay and others.

2.1.2 Transport Models

The prediction of reflux heat pipe transport capacity has received significant attention over the past several years, but there is as yet no satisfactory analytical model for this heat transfer device. It has been possible through dimensional analysis to establish empirical operating limits, and a summary of these models follows. This section closes with a comparison of each model with measured transport capacities for the 2.54 cm I.D. open core heat pipe described in Section 3.

A substantial number of the capacity models for vertical reflux operation liken the failure of a reflux heat pipe to the phenomena called "flooding" in the chemical process industry. In flooding, the falling annular film develops surface waves which grow to the point that the entire wave is blown back towards the condenser leading to evaporator dry-out.

Wallis Model

Wallis et al[13,14] assumed that the critical mass flow was related to a balance between gas inertial forces and hydrostatic forces, and that the critical axial heat flux density Q_{aw} for turbulent flow in both phases was given by

$$Q_{aw} = \frac{h_{fg} C_w^2 \sqrt{gD(\rho_\ell - \rho_v)\rho_v}}{\left(1 + \left(\frac{\rho_v}{\rho_\ell}\right)^{1/4}\right)^2} \qquad (W/cm^2) \qquad (2.1\text{-}1)$$

where D is the characteristic dimension of the heat pipe evaporator/adiabatic cross section, h_{fg} is the latent heat of vaporization, and ρ_ℓ and ρ_v are the liquid phase and vapor phase densities, respectively. The constant C_w is a constant that is less than or equal to 1.0, the exact value depending on end effects associated with the transition between evaporator and condenser. For a large condenser-to-evaporator cross-section ratio and a sharp-edged

transition, $C_w = 0.725$.[15] For heat pipes in which the wetting angle is close to zero and the evaporator and condenser have equal cross-sectional areas, the constant C_w may be very close to 1.0.

Kutateladze Model

The Wallis model does not account for surface tension effects or viscosity effects. A second approach to modeling flooding has used the Kutateladze number, which expresses the balance between surface tension, hydrostatic, and inertial forces,

$$C_k = K_v^{1/2} + K_\ell^{1/2} \tag{2.1-2}$$

where

$$K_v = \rho_v^{1/2} j_v / [g\sigma(\rho_\ell - \rho_v)]^{1/2} ; \tag{2.1-3}$$

$$K_\ell = \rho_\ell^{1/2} j_\ell / [g\sigma(\rho_\ell - \rho_v)]^{1/2} ; \tag{2.1-4}$$

and where j_v and j_ℓ are the volumetric flows of vapor and liquid per unit cross-sectional area, and σ is the surface tension.

Solving (2.1-2) for the case in which the mass flows of vapor and liquid are equal, the critical heat flux density is found to be

$$Q_{ak} = \frac{h_{fg} C_k^2 \left(\rho_v^2 g\sigma(\rho_\ell - \rho_v)\right)^{1/2}}{\left(1 + \left(\frac{\rho_v}{\rho_\ell}\right)^{1/2}\right)^2} \tag{2.1-5}$$

The theoretical value of C_k is $\sqrt{3.2}$. The Wallis and Kutateladze models of critical flux are not independent, since the ratio of (2.1-1) to (2.1-5) is

$$\frac{Q_{aw}}{Q_{ak}} = \left(\frac{C_w}{C_k}\right)^2 \sqrt{Bo} \qquad (2.1\text{-}6)$$

where the quantity in the square root is the Bond number, i.e., the ratio of hydrostatic-to-surface-tension forces,

$$Bo = [D^2 g(\rho_\ell - \rho_v)/\sigma]^{1/2} \qquad (2.1\text{-}7)$$

Composite Models

Wallis and Makkenchery[14] and Tien and Chung[16] recognized the fact that Q_{ak} is a phenomenologically more appropriate limit for large heat pipes where enclosure effects disappear while Q_{aw} is more appropriate for small tubes where the volume per unit contact area is much less. Tien and Chung modified C_k for use in equation (2.1-5) as follows to bridge the gap between the two models:

$$C_{kt} = C_k \bullet \tanh\left(0.5\ Bo^{1/2}\right) \qquad (C_k = \sqrt{3.2}) \qquad (2.1\text{-}8)$$

In the limit of small Bond numbers, when the modified Kutateladze number C_{kt} is substituted into (2.1-5), the resulting flux limit is of the Wallis form [equation (2.1-1)], while for large Bond numbers, C_{kt} tends towards C_k and the critical flux tends towards the Kutateladze limit.

The modified Kutateladze number C_{kt} does not represent experimental data in the transition region as well as might be desired because of the sluggish response of equation (2.1-8) to Bo. A more satisfactory transitional Kutateladze number which also provides Q_{aw} for small Bo when substituted into (2.1-5) is

$$C_{ks} = C_k \bullet [1\text{-}EXP(-\alpha^2 Bo)]^{1/2} \qquad (2.1\text{-}9)$$

where $\alpha = (C_w/C_k)^2$.

A comparison of these models with a large body of experimental reflux tube and open thermosyphon data is given in Figure 2.1.3. The peak flux data have been ratioed with respect to equation (2.1-5), using C_{kt} from equation (2.1-8) and C_w equal to 0.725 and 0.9 in equation (2.1-9). The data are represented more accurately with the proposed empirical model

$$Q_{ak} = C_{ks}^2 h_{fg} [\rho_v^2 g\sigma(\rho_\ell - \rho_v)]^{1/4} \Big/ [1 + (\rho_v/\rho_\ell)^{1/4}]^2 \quad (W/cm^2) \qquad (2.1\text{-}10)$$

where

$$C_{ks}^2 = 3.2 \left[1 - EXP(-\alpha^2 Bo)\right]^{1/4} \qquad (2.1\text{-}11)$$

However, equation (2.1-10) and the Wallis critical flux model may be of questionable value for heat pipes having very small cross sections. It does not seem physically correct that the Bond number should become of negligible importance for small tubes, since this is the direction of increasing surface tension forces. Also, the models do not include any effects of liquid or vapor viscosity. A major justification for the use of equation (2.1-10) is that a large body of data is correlated quite well by this model.

Bezrodny et al

Bezrodny and Beloivan have reported correlations based on extensive reflux heat pipe data using water, ethyl alcohol, and Freon-12.[17] They found two flow modes for heat pipes in the 1 to 5 cm I.D. range--below a critical fluid fill of about 25% of the evaporator volume, the heat pipe would exhibit one heat flux limit, while a slightly larger fill would paradoxically result in a 20 to 25% lower capacity. This was attributed to a change from annular to slug flow at higher mass loadings creating a net decrease in returning condensate.

The correlations derived from these data by Bezrodny and Beloivan are based on a modified Kutateladze number, where the critical heat flux density Q_{ab} is

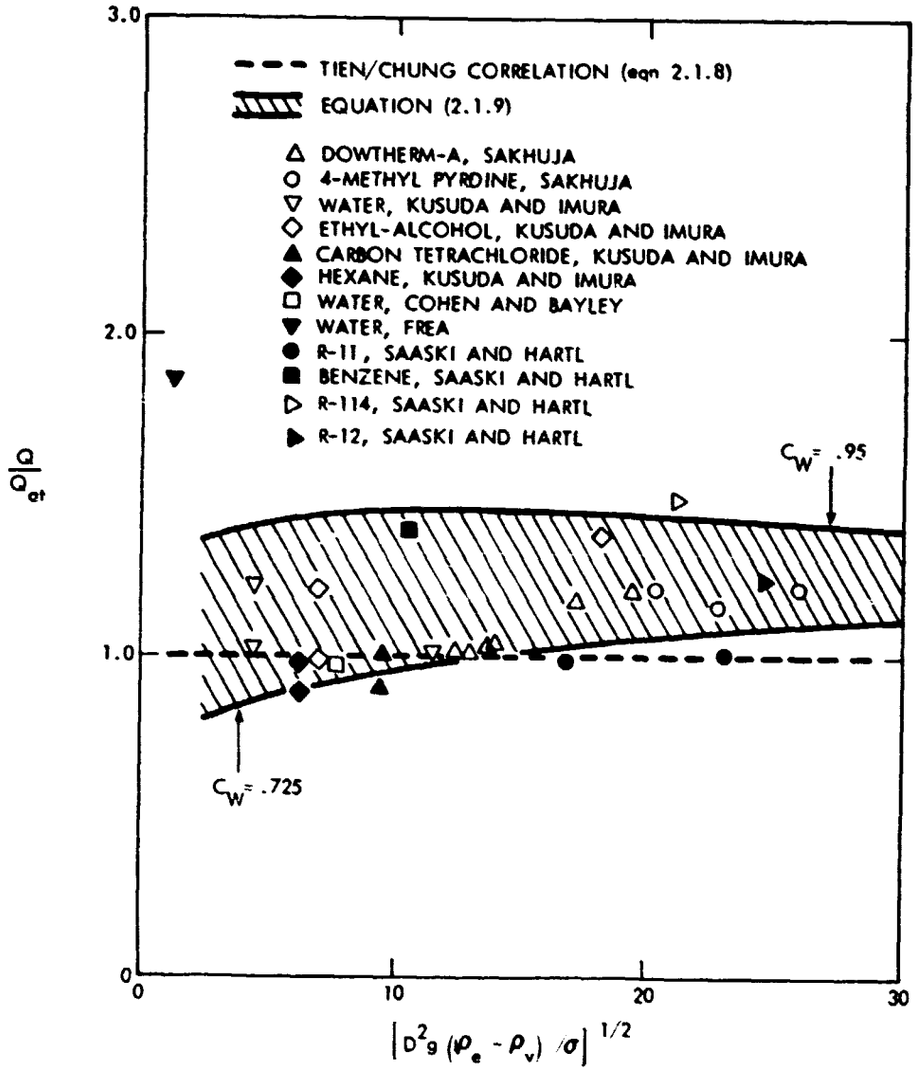

FIGURE 2.1.3. A COMPARISON OF FLOODING DRY-OUT DATA WITH TWO HYDRODYNAMIC MODELS.

$$Q_{ab} = C_{kb}^2 h_{fg} [\rho_v^2 g\sigma(\rho_\ell - \rho_v)]^{1/4} \quad (2.1\text{-}12)$$

and $$C_{kb}^2 = C_1 k_p^m \quad (2.1\text{-}13)$$

where $$K_p = P_s/[g\sigma(\rho_\ell - \rho_v)]^{1/4} \quad (2.1\text{-}14)$$

The modified Kutateladze number C_{kb} is dependent on the system saturation pressure P_s through a dimensionless pressure k_p, and falls in the following ranges depending on the value of K_p. For $5(10^3) \leq k_p \leq 5(10^4)$,

$$5.65/K_p^{0.13} \leq C_{kb}^2 \leq 6.02/K_p^{0.13} \quad (2.1\text{-}15)$$

For the higher pressure range $5(10^4) \leq K_p \leq 3.5(10^5)$, it was found that

$$1.35 \leq C_{kb}^2 \leq 1.6 \quad (2.1\text{-}16)$$

Bezrodny and Sakhatsh performed additional tests on tilted water heat pipes of 1.2 to 3.8 cm I.D.[18] Typical data are shown in Figure 2.1.4. The bistable operation discussed earlier at higher tilts is quite obvious. For the tilt angle θ in the range 5 to 30°, the data were correlated with the formula

$$Q_{ac} = 3300\, P_s^{1/4}\, \theta^{0.54} \ell_e^{0.44} \quad (W/cm^2) \quad (2.1\text{-}17)$$

with vapor pressure P_s in MPa and the length in meters.

Kusuda and Imura

Kusuda and Imura have developed a model for vertical reflux transport capacity that is based on a semi-empirical physical model rather than dimensional analysis.[19] A related approach is given in reference 19a. This relationship based on data gathered at 1 atmosphere vapor pressure, gives the critical heat flux density Q_{ac} for tubular heat pipes as

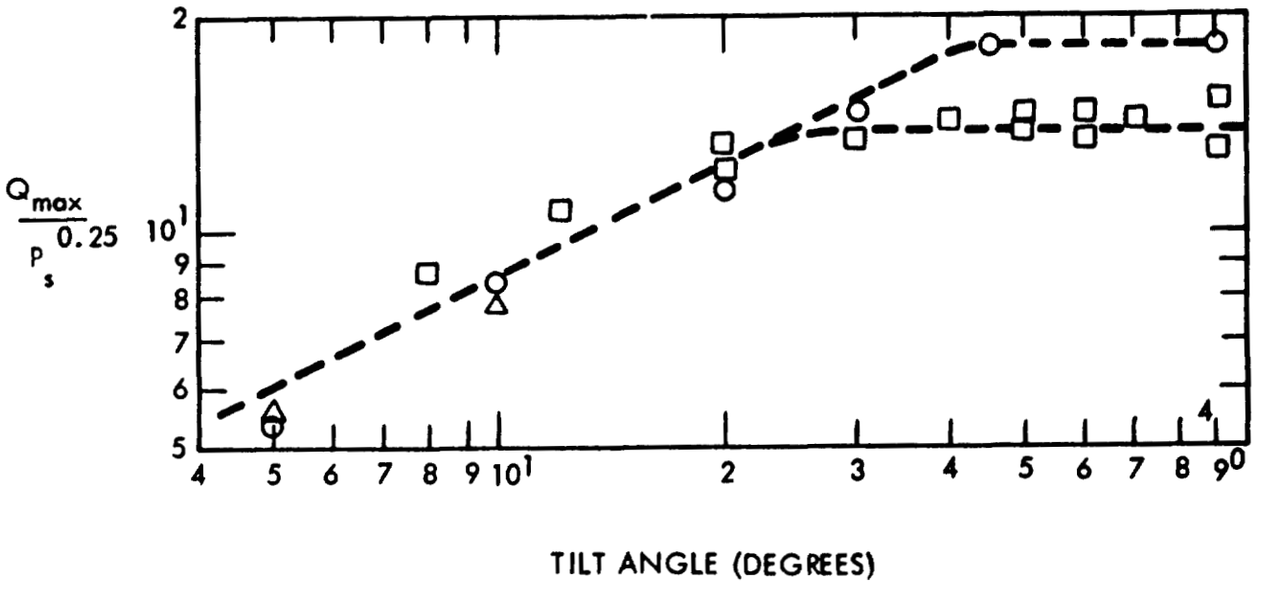

FIGURE 2.1.4. EFFECT OF TILT FROM HORIZONTAL ON REFLUX HEAT PIPES OF BEZRODNY AND SAKHATSH.

$$Q_{ac} = 0.4\ \rho_v h_{fg} \left(\frac{4\sigma^3 \rho_\ell^2 g}{\pi u_\ell \rho_v^4 D}\right)^{1/7} \left[1 + \frac{5}{4}\left(\frac{\rho_\ell}{\rho_v}\right)^{.8}\left(\frac{D}{L_e}\right)\left(\frac{C_{p\ell}\Delta T_s}{h_{fg}}\right)\right] \quad (W/cm^2) \qquad (2.1\text{-}18)$$

where D = heat pipe diameter, u = viscosity, h_{fg} = latent heat per unit mass, L_e = evaporator length, C_p = specific heat, and ΔT_s = condensate subcooling relative to the vapor core.

University of Stuttgart

Abhat, Nguyenchi, Groll, and others at the Institut für Kernenergetik have been studying smooth-wall and screened-wall reflux heat pipes and have published several papers on this work.[20-23] An important contribution of this work has been detailed study of the relationship between axial and radial heat flux limits. For short heat pipes operated with low vapor pressure fluids, the heat flux at the heat pipe surface may lead to film boiling or depriming prior to any axial heat flux limit being exceeded. Based on influence parameter studies of water-charged screened wick heat pipes, the following power-law relations have been found to describe dependence of limiting heat flux on system variables.[23]

+3.49 dependence on heat pipe O.D.
+0.727 on the fractional liquid fill of the evaporator
+0.424 dependence on sin θ_{tilt}
-0.404 dependence on evaporator length
-1.0 on total fluid volume

2.1.3 Comparison of Models

Figures 2.1.5 and 2.1.6 show the various models described in this section compared with experimental data gathered at this facility with the 2.54 cm I.D. reflux heat pipe shown in Figure 3.1.4. For these tests, the heat pipe core was open. The measured critical heat fluxes should be somewhat lower than the predicted values since heat pipe burnout was identified as the point at which the overall heat pipe conductance began to decrease, since the general data trend was an increasing overall conductance unless burnout was imminent.

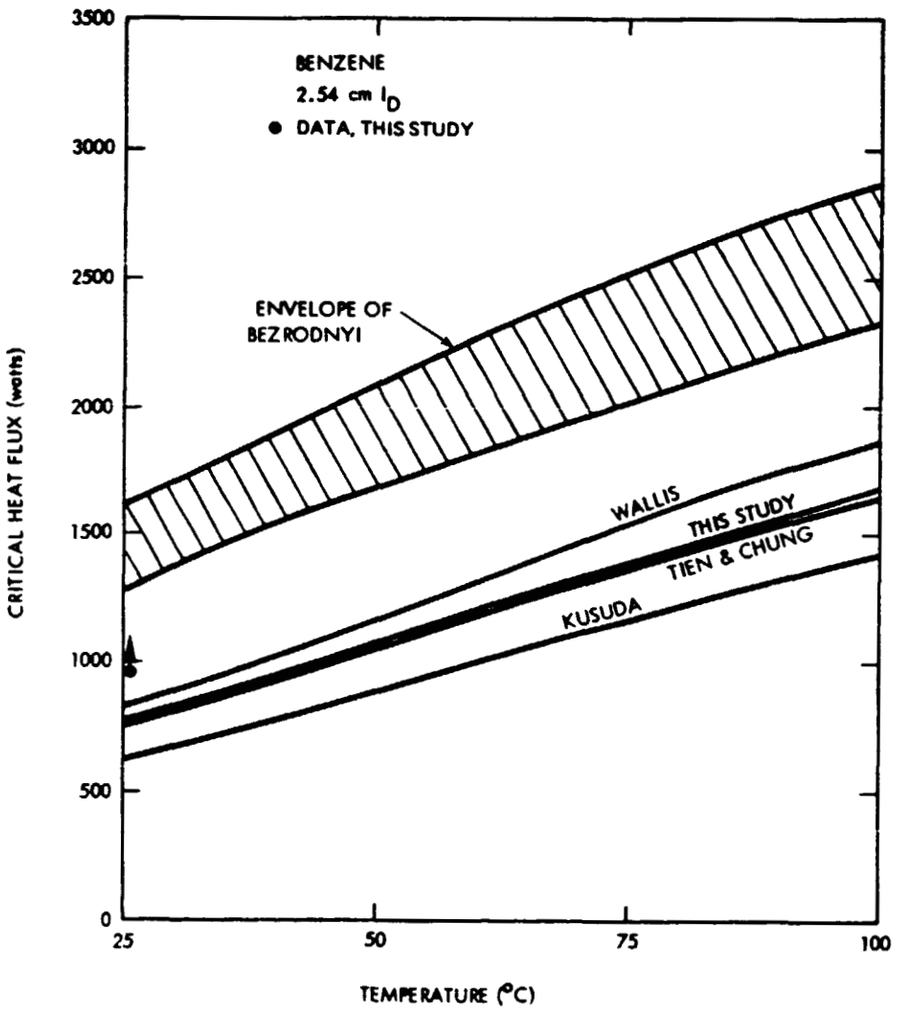

FIGURE 2.1.5. CRITICAL AXIAL HEAT FLUX PREDICTIONS FOR A 2.54 CM I.D. HEAT PIPE CHARGED WITH BENZENE.

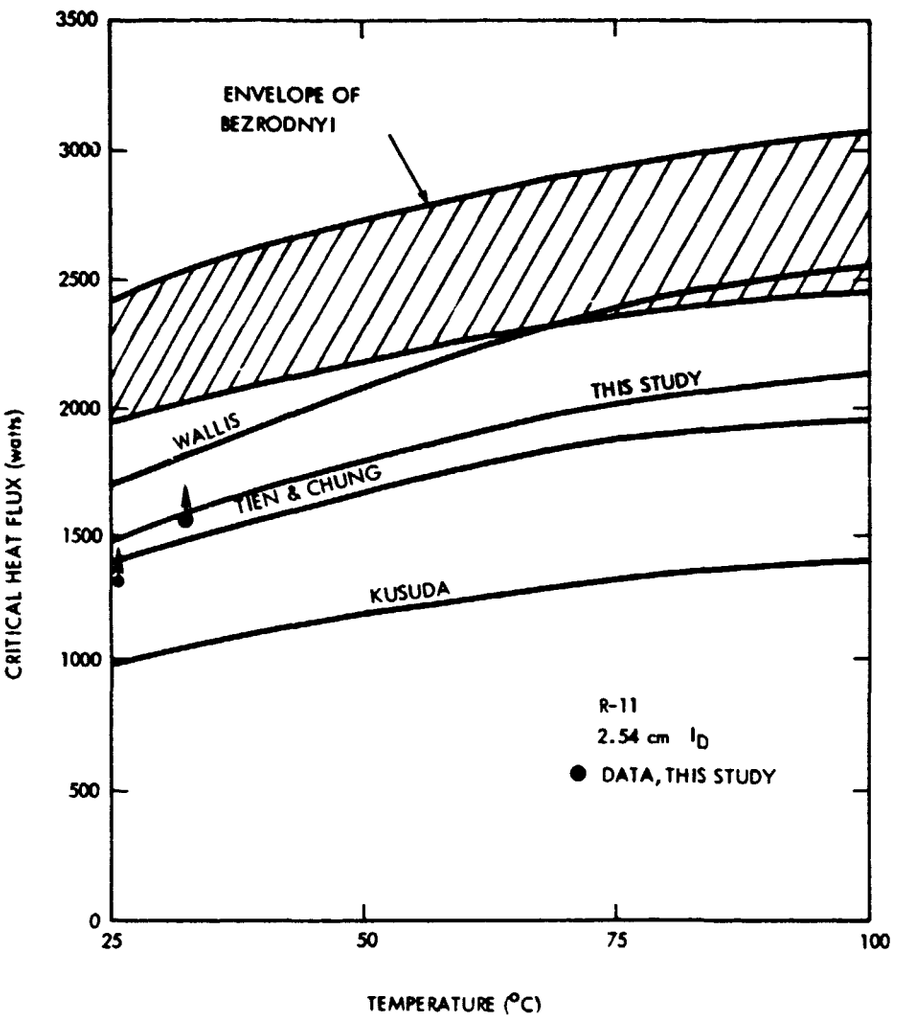

FIGURE 2.1.6. CRITICAL AXIAL HEAT FLUX PREDICTIONS FOR A 2.54 CM I.D. HEAT PIPE CHARGED WITH R-11.

In the case of benzene, the burnout was very rapid, with a sharp reduction in conductance, while with R-11, the conductance would often decrease gradually so that burnout was difficult to identify. The data agrees well with equation (2.1.9) if C_w is assumed to be in the range $0.7 \leq C_w \leq 0.95$.

2.1.4 Transport Requirements

Up to this time, the application of heat pipes to heat recovery has been primarily in the area of air-to-air recuperators. Heat from exhausting hot gases (such as from furnaces, ovens, dryers, incinerators, gas turbines, stale building air, etc.) is reclaimed and used to heat incoming cold air as described in Section 2.1. In many of these air-to-air applications where the overall temperature difference between the hot and cold streams is small, the performance of the heat exchanger is primarily limited by the thermal resistances associated with the finned exteriors. As the temperature difference between the two streams increases, however, it is possible to exceed either the internal surface vaporization limit of the heat pipe or its axial transport capacity. These limits will also be approached with greater frequency when the heat pipe is used in situations where exterior heat transfer coefficients are larger, such as in air-to-fluid, liquid-to-air, or liquid-to-liquid heat recovery applications.

Various correlations exist for heat transfer coefficients associated with air-to-air finned tube heat exchangers.[24-26] An empirical model for triangular-pitch heat exchangers that has been found to be reasonably accurate is that of Briggs and Young,[24]

$$h = \frac{0.1378\ Re^{0.718} Pr^{1/3} K_a (S/L)^{0.296}}{D_r} \qquad (W/cm^2K) \qquad (2.1\text{-}19)$$

where $Re = D_r G_m / u_a$.

The Reynolds number Re is based on the O.D. of the tube, D_r, the mass flow rate per unit area at minimum heat exchanger cross section, G_m, and the gas viscosity, u_a. The heat transfer coefficient is, in addition, dependent on the Prandtl number, Pr, the air gap between fins, S, the fin length, L, and the air conductivity, K_a. The exterior conductance per unit length of a 2.54 cm O.D. heat pipe with L = 1.27 cm is shown in Figure 2.1.7 for fin densities of 2.36 cm^{-1} and 4.72 cm^{-1} (neglecting heat transfer to the tube itself). For each fin density, a range of conductances is shown that corresponds to a fin thickness span of 0 to 0.10 cm. Table 2.1.1 summarizes the radial heat flux densities and axial heat fluxes per unit evaporator length for typical flue gas velocities and various gas-metal temperature differences. The lower end of the temperature difference range is indicative of air conditioning applications, the middle temperature differences are indicative of industrial air-to-air recuperators, while the upper end is indicative of air-to-liquid systems for the preheating of process fluids by flue gases.

Typical evaporative heat flux densities for low temperature difference applications range from less than 1 to about 2 W/cm^2. Axial heat flux requirements range from several hundred to less than 2000 watts per meter of evaporator length. Industrial air-to-air recuperator-type applications show evaporative heat flux densities in the range of 2 to 15 W/cm^2 and axial heat fluxes of a few thousand watts to more than 10 kilowatts per meter of evaporator. Air-to-liquid applications show heat flux densities from about 5 to 25 $watts/cm^2$ and axial fluxes from several thousand watts/m to almost 20 kW/m.

Most of Dowtherms, organic, and halocarbon working fluids show axial reflux transport limits for a 2.54 cm I.D. that are in the range of 1000 to 2500 watts. It is therefore difficult to apply conventional reflux heat pipes to heat recovery applications where the driving temperature differences are large, such as stack gas recuperators, and/or where the evaporators are longer than about 1 meter. A similar or worse state of affairs is found for liquid/liquid or liquid/two-phase process streams where the heat transfer coefficients are substantially larger than those found with forced-air and finned-tube systems.

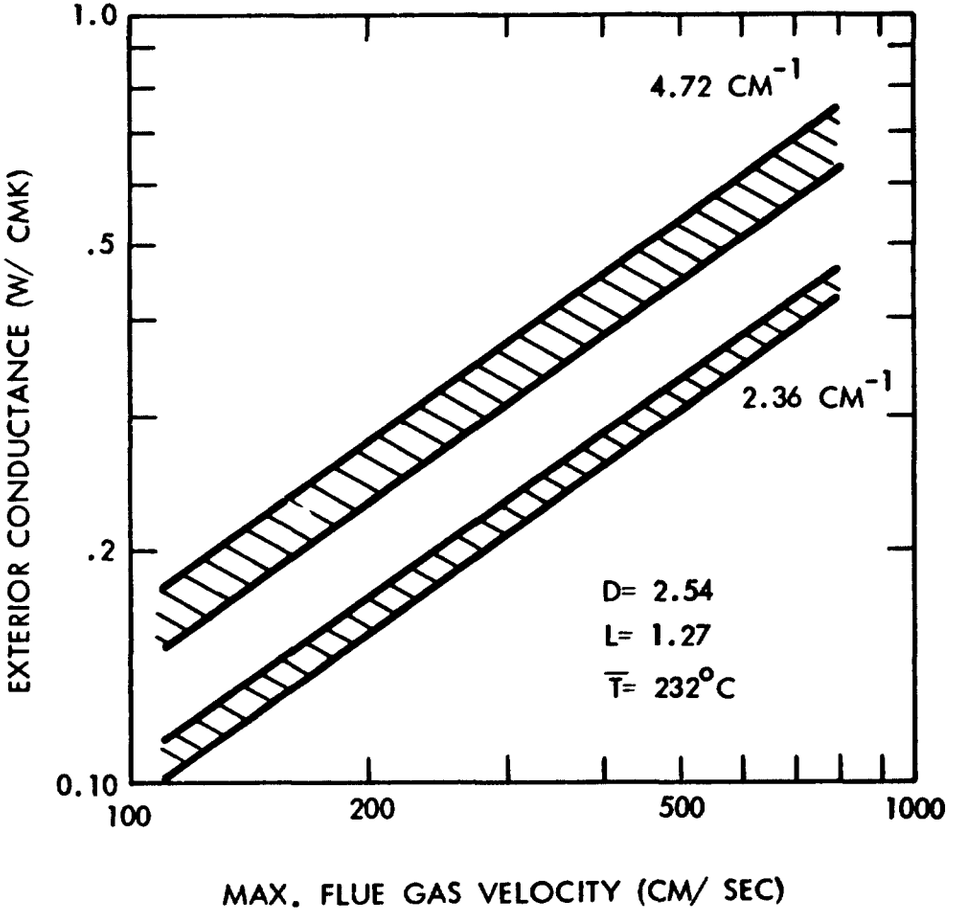

FIGURE 2.1.7. CONDUCTANCE PER UNIT TUBE LENGTH FOR A FINNED TUBE IN CROSS FLOW FOR FIN DENSITIES OF 2.36 CM^{-1} AND 4.72 CM^{-1}.

TABLE 2.1.1. HEAT FLUX REQUIREMENTS FOR AIR-TO-AIR HEAT RECOVERY HEAT PIPES(1)

Maximum Gas Velocity (cm/sec)	Air-to-Fin Temperature Difference (K)	Radial Flux Densit/ (W/cm^2)		Per Unit Length Axial Heat Flux (W/M)	
		2.36 fins/cm	4.72 fins/cm	2.36 fins/cm	4.72 fins/cm
200	19	0.4	0.6	300	500
	111	2.3	3.6	1,800	2,900
	167	3.4	5.4	2,700	4,300
	278	5.7	9.0	4,600	7,100
500	19	0.8	1.2	600	900
	111	4.4	6.9	3,500	5,500
	167	6.7	10.4	5,300	8,300
	278	11.1	17.3	8,800	13,800
750	19	1.0	1.6	800	1,300
	111	5.9	9.2	4,700	7,400
	167	8.9	13.9	7,100	11,100
	278	14.8	23.1	11,800	18,500

(1) Heat pipe O.D. = 2.54 cm; fin length L = 1.27 cm;
Average air film temperature $\bar{T}$ = 232 °C;
Fin width = 0.05 cm; fin effectiveness = 100%.

From an economic standpoint, it is further clear that to achieve a given level of overall system conductance for a heat pipe heat exchanger, it is more desirable to increase the length of each heat pipe than to install more heat pipes, but this direction of economic optimization is restricted by the axial transport limit. To expand the use of heat pipes to more varied heat recovery applications, it is necessary to develop methods of maximizing heat pipe radial and axial heat flux limits and evaporative and condensation heat transfer coefficients.

2.2 Cocurrent Flow Heat Pipe

As discussed in Section 2.1, the primary factor limiting transport capacity in conventional gravity reflux heat pipes is the countercurrent vapor-liquid shear process that results in liquid starvation of the evaporator and substantial flooding of the condenser surface. To reach heat flux levels beyond this capacity limit, a class of heat pipes has been investigated and modeled that operate completely in cocurrent two-phase flow. This is accomplished by forming what is essentially an optimized "thermosyphon boiler" within the heat pipe. The general configuration studied is shown in Figure 2.2.1.

In the evaporator and adiabatic, condensate is separated from the turbulent two-phase mixture produced by boiling by a sheath of impermeable material. For most purposes, this sheath is simply a thin-walled tube. The tube is open at the lower end and may have an optional slot or set of bleed holes along the length in the evaporator to (a) more uniformly wet the evaporator I.D. and (b) reduce the overall pressure drop attributable to condensate return. Liquid in the condensate tube does not generally boil except at very low heat flux levels, and for all practical purposes, it can be assumed that the condensate subcooling is more than adequate to forestall a condensate flow reversal.

In the condenser, the heat pipe cross section has been divided into halves by a tight-fitting separator plate that extends to within a few diameters of the blind end of the condenser. At the adiabatic-condenser interface, the separator plate and condensate return tube are coupled together so as to direct

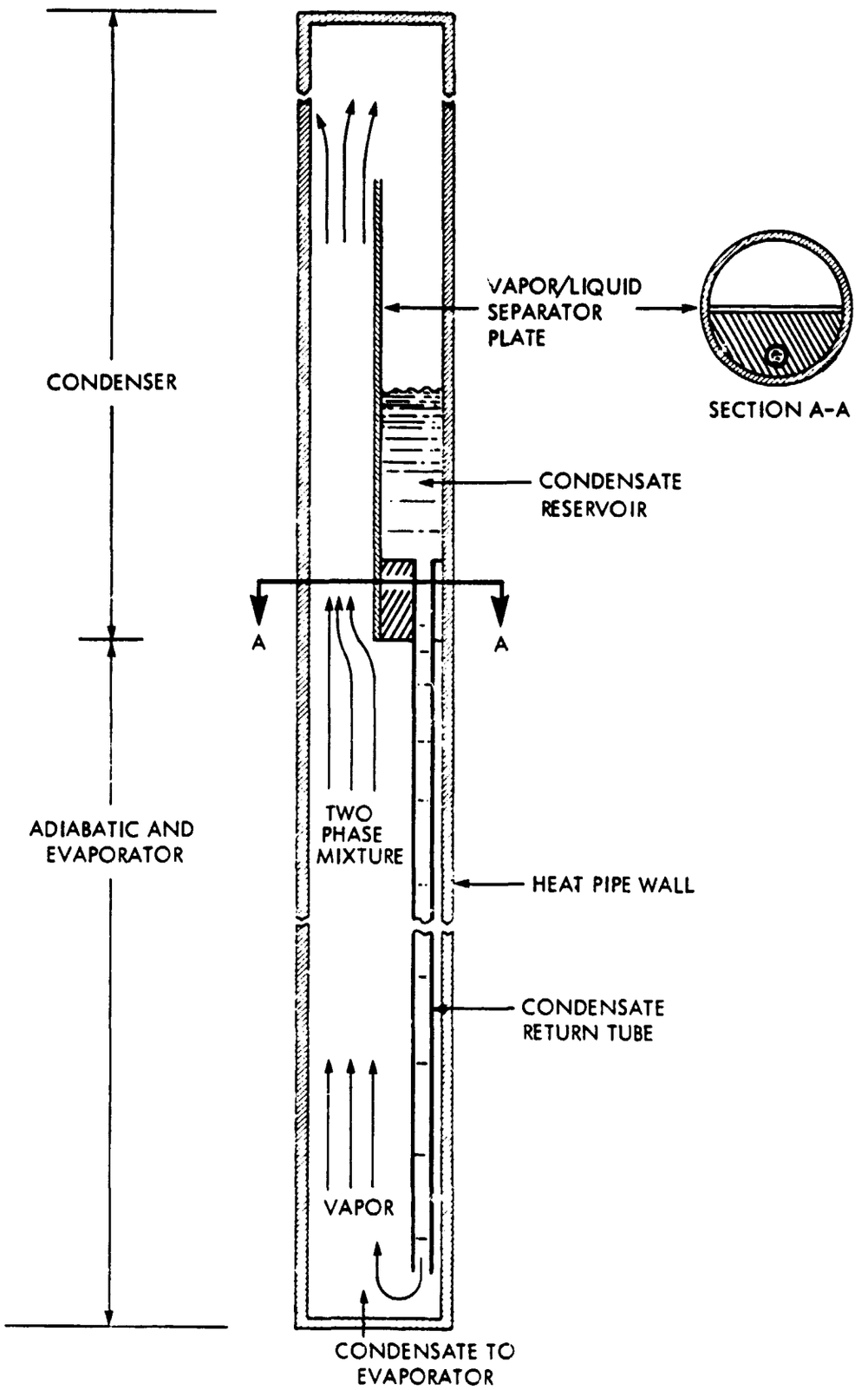

FIGURE 2.2.1. HIGH PERFORMANCE REFLUX HEAT PIPE.

and transport condensate back to the evaporator from one of the condenser half-sections. The condensing two-phase flow executes a hairpin-shaped flow pattern in the condenser that shears stagnant condensate from the condensing surfaces and sweeps it towards the return tube interface. The condenser section that is joined hydraulically to the condensate tube partially fills with liquid and serves as a reservoir or hydraulic capacitor, reducing the slugging and oscillatory behavior often seen in open-section reflux boilers, while the high velocity flow created by the separator enhances the condensing heat transfer coefficient by reducing condensate film thickness. The high velocity cocurrent flow also minimizes liquid puddling and reduces the liquid load necessary to sustain a given mass transport rate.

A benefit deriving from this type of reflux heat pipe, in addition to high heat flux rates, is a substantial body of relevant analytical and empirical studies of cocurrent flow that are of use in modeling and optimization.

2.2.1 Theory: Cocurrent Flow Heat Pipe

Operation of a heat pipe configured as in Figure 2.2.1 has been modeled primarily on the two-phase pressure drop expressions developed by Lockhart and Martinelli[27] and by Owens.[28] The transport capacity is found by determining the mass flow rate at which the available hydrostatic head difference between the "up" leg and the "down" leg of the flow circuit is balanced by the frictional and acceleration pressure drops associated with the two legs,

$$\Delta P_g = \Delta P_a + \Delta P_f , \qquad (2.2\text{-}1)$$

where ΔP_g is the available hydrostatic head, ΔP_a is the pressure drop resulting from fluid acceleration, and ΔP_f is the pressure drop resulting from friction. The "up" leg of the flow circuit in Figure 2.2.1 includes the evaporator and adiabatic core sections surrounding the condensate tube and the half-section of the condenser with upward two-phase flow. The "down" leg includes the condenser half-section in which the working fluid flow is downward and the inner core of the condensate return tube.

The variou pressure drops associated with this cocurrent flow heat pipe are diagrammed in Figure 2.2.2 and are as follows:

Evaporator (upflow)

- frictional pressure drop, R_{ef}
- acceleration pressure drop, R_{ea}

Adiabatic (upflow)

- frictional pressure drop--prior to separator plate, R_{af}
- frictional pressure drop--with separator plate, R_{asf}
- constriction pressure drop--with separator plate, R_{asc}

Condenser (upflow and downflow)

- frictional pressure drops, R_{cuf} and R_{cdf}
- deceleration pressure differences, R_{cua} and R_{cda}
- expansion and constriction pressure drops at the condenser end of separator plate, R_{cue} and R_{cdc}

Condensate Return Tube (downflow)

- frictional pressure drop, R_{tf}
- expansion and constriction pressure drops, R_{te}, R_{tc}

The following sections outline the methods used for calculating each flow resistance.

In the subsequent analyses, all or most of the flow cross sections are assumed noncircular, and it is necessary to use the hydraulic radius approximation for the calculation of Reynolds numbers and friction pressure drops. The expressions below are used extensively in the hydrodynamic modeling of heat pipe function that follows.

$$-\left(\frac{dp}{dz}\right) = \frac{F\left(Re_h\right)}{R_h}\left(\frac{1}{2}\rho v_{av}^2\right) \qquad (2.2\text{-}2)$$

$$Re_h = \frac{4R_h \rho v_{av}}{u} = \frac{4\dot{m}}{uP_w}$$

$$R_h = A_p/P_w$$

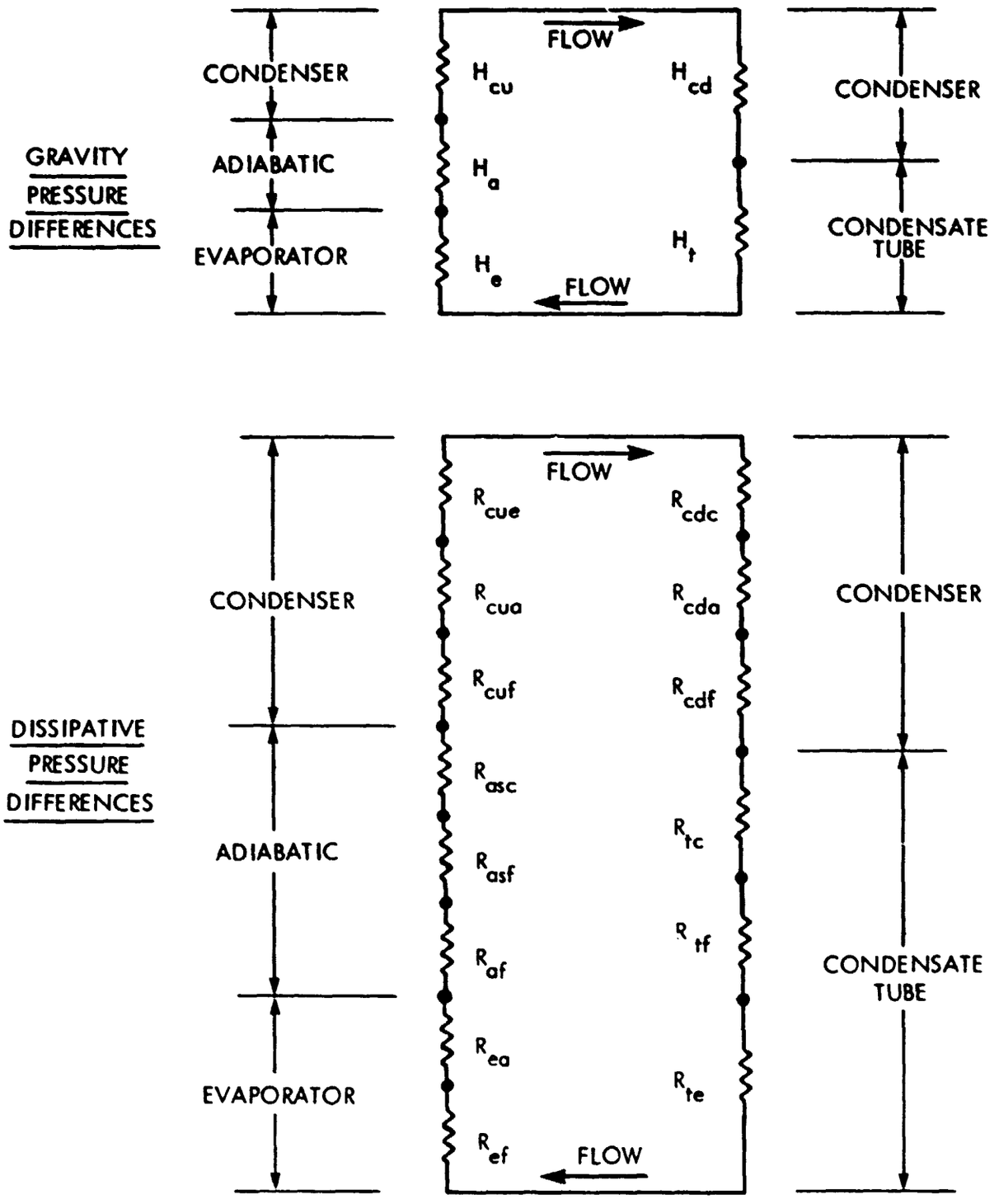

FIGURE 2.2.2. GRAVITY HEADS (H_i) AND PRESSURE DROPS (R_i) ACCOUNTED FOR IN THIS MODEL OF AN OPERATING COCURRENT FLOW HEAT PIPE.

where R_h is the hydraulic radius, P_w is the wetted perimeter, A_p is the perpendicular flow area, $\dot{m}$ is the mass flow rate, v_{av} is the mean flow velocity, ρ is the fluid density, u is the fluid viscosity, and F is the Fanning friction factor, which is a function of Re_h.

For Reynolds numbers less than 2000, the friction factor is given by

$$F = 16/Re_h \qquad (2.2\text{-}3)$$

For Reynolds numbers in the range $2000 < Re < 2.5\ (10^6)$, the friction factor expression used is for hydraulically smooth tube, and agrees with Prandtl's universal law of friction[29] to within ±0.5%,

$$F = \frac{0.219622}{Re_h^{0.43}} - 0.261297\ (10^{-3})\ \ln\ (Re_h) + 5.95156\ (10^{-3}) \qquad (2.2\text{-}4)$$

2.2.1.1 Evaporator

For the evaporator, the pressure drops R_{ef} and R_{ea} were calculated using the homogeneous two-phase flow model of Owens[28].

In reference 28, Owens presents an analytical model for the pressure drop in homogeneous two-phase flow that compares favorably with experimental data for air-water mixtures from 14.7 psia to 3000 psia with qualities of about 10 to 100%, and for vaporizing flows of water ranging from 64 to 381 psia with qualities up to 57 percent. If the quality "x" of the vaporizing flow changes linearly with axial evaporator position, and if both the liquid and vapor densities and $d\rho_v/dP$ are essentially constant, then the evaporator pressure drop $R_{ef} + R_{ea}$ is

$$R_{ef} + R_{ea} = -\frac{1}{B} \cdot \ln\left(\frac{1 + Bx_1}{1 + Bx_o}\right)\left[\frac{\ell_e}{(x_1 - x_o)}\left(\frac{dP}{dz}\right)_o \cdot \left(1 - \frac{A}{B}\right) - AC\right]$$

$$- \frac{\ell_e A}{B}\left(\frac{dP}{dz}\right)_o \qquad (\text{dynes/cm}^2) \qquad (2.2\text{-}5)$$

where $A = \rho_\ell/\rho_v - 1$; $B = G_e^2\, d(1/\rho_v)/dP$; $C = G_e^2/\rho_\ell$, where ℓ_e is the evaporator length, G_e is the total mass flow per unit cross-sectional area; x_o and x_1 are the mixture qualities at the evaporator entrance and exit, respectively, and (dP/dz) is the pressure gradient at the blind end of the evaporator, z = 0, with the flow assumed to be completely liquid, i.e., zero quality.

The pressure gradient term $(dP/dz)_o$ is not calculated directly, but is instead calculated from the pressure gradient at the evaporator exit. This insures a consistent pressure gradient transition at the evaporator-adiabatic interface. This gradient term is calculated as follows.

Owens shows that the friction factor for two-phase flow is very nearly equal to the friction factor that would be used if the mixture were all in the liquid state, having zero quality. Hence, the frictional pressure drop in two-phase flow, $-(dP/dz)_{tpf}$, is approximately the product of an arithmetic constant and a term involving the mean density,

$$-\left(\frac{dP}{dz}\right)_{tpf} \simeq \frac{F_\ell G_e^2}{2\rho_\ell R_h}\left[1 + X_i\left(\frac{\rho_\ell}{\rho_v} - 1\right)\right] \tag{2.2-6}$$

$$= \text{const.} \times \left[1 + X_i\left(\frac{\rho_\ell}{\rho_v} - 1\right)\right] \tag{2.2-7}$$

where F_ℓ is the liquid-state friction factor, X_i is the average local mixture quality, and R_h is the evaporator hydraulic radius. Equation (2.2-6) would be exact if F_ℓ were replaced by the unknown two-phase friction factor, F_{tp}. The best constant for (2.2-7) to achieve continuities at the evaporator/adiabatic interface is found by calculating the frictional pressure gradient at the evaporator exit using the Lockhart-Martinelli correlation.

$$\text{const.} = -(dP/dz)_{z=\ell_e} \div \left[1 + X_1\left(\frac{\rho_\ell}{\rho_v} - 1\right)\right] \tag{2.2-8}$$

2.2.1.2 Adiabatic

Two-phase pressure drops in the adiabatic and separator sections have been modeled using the empirical correlation of Lockhart and Martinelli.[27]

With this method of estimating two-phase pressure drop, the pressure drop is given by either a vapor phase pressure drop multiplied by a correction factor

$$\Delta P_{tp} = R_{af} = Y_v^2 \bullet (dP/dz)_{vs} \bullet \ell_a \qquad (\text{dynes/cm}^2) \qquad (2.2\text{-}9)$$

where ℓ_a is the length of the adiabatic section, ΔP_{tp} is the two-phase pressure drop, $(dP/dz)_{vs}$ is the pressure gradient if only the gas were flowing through the heat pipe cross section, and Y_v^2 is a correction factor dependent on the ratio of the single-phase liquid to single-phase vapor pressure gradient.

$$Y_v^2 = f(\underline{X}) \qquad (2.2\text{-}10)$$

where $\underline{X}^2 = (dP/dz)_{\ell s} \Big/ (dP/dz)_{vs}$.

In the term $\underline{X}^2$, $(dP/dz)_{\ell s}$ is analogous to $(dP/dz)_{vs}$ in that it is the pressure gradient that would result if only the liquid phase were flowing through the heat pipe.

The value of the parameter Y_v^2 also depends on whether the single-component partial flows are laminar or viscous on the basis of the respective Reynolds numbers. If both partial flows have Reynolds numbers greater than 2000, the function Y_v^2 is given to within ±5% over the range $0.01 < X < 100$ by

$$Y^2 = \left(1 + \underline{X}^{0.3616}\right)^{1.01705} \left(1 + \sqrt{\underline{X}}\right)^{3.15712} \qquad \begin{matrix}(\text{turbulent vapor,} \\ \text{turbulent liquid})\end{matrix} \qquad (2.2\text{-}11)$$

For liquid-phase Reynolds numbers less than 2000, the function Y_v^2 is given over the same range to within ±8% by

$$Y_v^2 = \left(1 + 1.125\underline{X}^{1.5}\right)^{0.218215} \cdot \left(1 + \sqrt{\underline{X}}\right)^{3.31326} \qquad \begin{matrix}\text{(turbulent vapor,} \\ \text{viscous liquid)}\end{matrix} \qquad (2.2\text{-}12)$$

The vapor phase is assumed to be in turbulent flow at all times.

The frictional pressure drop R_{asf}, which must be considered when the separator plate extends into the adiabatic, is calculated using a procedure identical to that above.

The constriction pressure drop associated with the transition from the adiabatic to the half-section is calculated assuming an abrupt transition,[30]

$$R_{asc} = \left(\frac{G_s^2\,(1 + AX_1)}{2\rho_\ell}\right) \cdot 0.45 \left(1 - \frac{A_s}{A_a}\right) \qquad (\text{dynes/cm}^2) \qquad (2.2\text{-}13)$$

where G_s is the mass flow rate per unit area of separator cross-sectional area, A_a and A_s are the flow cross sections in the adiabatic and separator sections respectively, and "A" is given in the nomenclature for equation (2.2-5).

2.2.1.3 Condenser

For all design cases, it is assumed that the separator plate ends at the condenser entrance or penetrates into the condenser for some finite fraction of the condenser length, and that the condensation process occurs uniformly throughout the condenser. As a result of visual observations of heat pipe operation using a glass adiabatic section, the separator plate is found *not* to be completely successful in separating the countercurrent flows within the condenser. The upward flowing two-phase mixture can entrain substantial amounts of condensate through the two slots formed by a loose-fitting separator plate. To account for this leakage, the condenser inlet quality X_2 is a user-modifiable variable. The exit quality X_5 is also an input variable, although under normal conditions of fluid charge, X_5 can be assumed equal to zero.

The frictional and acceleration pressure changes in the condenser are calculated using the same homogeneous flow model as in the evaporator. However, because of mixture deceleration associated with condensation, there is some pressure recovery to compensate for frictional loss. This partial pressure recovery will always occur in a zone with decreasing quality.

With a uniform condensation rate, the quality of the mixture in the condenser is assumed to change linearly with axial position with the axial rate-of-change doubling once the vapor-liquid mixture exits the first condenser half-section. Therefore, the two-phase qualities on opposite sides of the separator plate are generally substantially different, even where the upward- and downward-moving flows meet at the separator plate exit. These qualities at the separator plate exit, X_3 and X_4, are given by

$$X_3 = X_2 + (X_5 - X_2) \frac{\ell_{sc}}{2\ell_c} \tag{2.2-14}$$

and

$$X_4 = X_5 - (X_5 - X_2) \frac{\ell_{sc}}{2\ell_c} \tag{2.2-15}$$

where ℓ_{sc} is the penetration depth of the separator plate in the condenser, and ℓ_c is the condenser length.

The pressure drop terms R_{cuf}, R_{cua}, R_{cdf}, and R_{cda}, are calculated using equation (2.2-5) with the two-phase qualities, section length, and initial pressure drops characteristic of the two condenser half-sections.

The outlet and inlet constriction resistances R_{cue} and R_{cdc} associated with the termination of the separator plate in the condenser have been each approximated as the pressure drop associated with a 90° mitered corner.[31]

$$R_{cue} = \frac{G_c^2\left(1 + AX_3^{\cdot}\right)}{2\rho_\ell}\left(60\ F_{c\ell}\right) \qquad \text{(dynes/cm}^2\text{)} \qquad (2.2\text{-}16)$$

$$R_{cdc} = \frac{G_c^2\left(1 + AX_4\right)}{2\rho_\ell}\left(60\ F_{c\ell}\right) \qquad \text{(dynes/cm}^2\text{)} \qquad (2.2\text{-}17)$$

where G_c is the mass flow per unit area on either side of the condenser separator plate, and $F_{c\ell}$ is the friction factor for flow on either side of the separator plate, assuming all mass flow to be in the liquid state,

$$F_{c\ell} = F\left(4\ \dot{m}_c/u_\ell P_{wc}\right) \qquad (2.2\text{-}18)$$

where $\dot{m}_c$ is the condenser total mass flow rate, and P_{wc} is the wetted perimeter on either side of the separator plate.

2.2.1.4 Condensate Tube

The frictional pressure drop in the condensate return tube, R_{tf}, is calculated using equation (2.2-2),

$$R_{tf} = \frac{F_t}{R_h}\left(\frac{G_a^2}{2\rho_\ell}\right)\ell_t \qquad \text{(dynes/cm}^2\text{)} \qquad (2.2\text{-}19)$$

where F_t is the condensate tube friction factor, R_h is the tube hydraulic radius, and ℓ_t is the condensate tube length.

The constriction resistance R_{tc} at the condensate tube-separator interface is given by

$$R_{tc} = \frac{G_t^2}{2\rho_\ell} \cdot 0.45\left(1 - \frac{A_t}{A_x}\right) \qquad (2.2\text{-}20)$$

where G_t is the mass flow per unit area in the condensate tube, A_t is the condensate tube flow cross section, and A_x is the flow cross-sectional area on one side of the separator.

The expansion resistance R_{te} represents the pressure difference arising from flow exiting the condensate tube of area A_o into the total evaporator cross section and thereafter being diverted 180° and constricted down to a smaller area A_1 that is equal to the cross-sectional area of the evaporator minus the tube cross-sectional area. This multiple effect flow resistance has been approximated as the sum of

(1) An expansion from area A_o to area $(A_o + A_1)$.
(2) Two 90° mitre bend of cross-sectional area $(A_o + A_1)$.
(3) A constriction from area $(A_o + A_1)$ to area A_1.

Employing expansion coefficients in references 30 and 31, the pressure drop is

$$R_{te} = \frac{G_t^2}{2\rho_\ell} \left(\frac{1 + 120\ B^2 F_e}{(1 + B)^2} + \frac{0.45\ B^3}{1 + B} \right) \qquad (2.2\text{-}21)$$

where G_t is the mass flow per unit area in the condensate tube, $B = A_o/A_1$, and F_e is the friction factor based on the Reynolds number $Re = 4m/[u_\ell(P_{wl} - P_{wo})]$, where m is the total mass flow, u is the liquid viscosity and P_{wl} and P_{wo} are the wetted perimeters of the evaporator and condensate tube, respectively.

2.2.1.5 Hydrostatic Pressure Difference

The driving pressure difference for fluid circulation is the difference in hydrostatic head between the "up" leg of the heat pipe and the "down" leg. The various gravity pressure differences are shown in Figure 2.2.1 as H_i. The gravity pressure differences for the evaporator and condenser sections of the heat pipe are calculated using the expression derived by Owens for a homogeneous mixture. This expression is, for the evaporator gravity head H_e,

$$H_e = \frac{g\rho_\ell \ell_e \sin\theta}{(B - A)(X_1 - X_o)} \left[\ell n \left(\frac{1 + BX_1}{1 + BX_o} \right) + \ell n \left(\frac{1 + AX_o}{1 + AX_1} \right) \right] \qquad (2.2\text{-}22)$$

where B and A have been previously defined for equation (2.2.5), and θ is the angle of the heat pipe axis with respect to horizontal. For the condenser heads H_{cu} and H_{cd}, ℓ_e will be replaced in equation (2.2-22) by the length of the separator plate in the condenser, ℓ_{sc}, G_e will be replaced in "B" by G_c, and the entrance and exit qualities X_o, X_1 will be replaced with either X_2, X_3 or X_4, X_5.

In the adiabatic zone and the vapor-phase side of the separator section in the adiabatic, the gravity head H_a is given by

$$H_a = \rho_\ell g \ell_z \sin\theta/(1 + AX_1) \qquad (2.2\text{-}23)$$

The gravity head for the condensate tube is

$$H_t = \rho_\ell g \ell_t \sin\theta \qquad (2.2\text{-}24)$$

In these expressions, ℓ_a and ℓ_t are, respectively, the lengths of the adiabatic and the condensate tube. If the condensate reservoir shown in Figure 2.2.1 fills up substantially, ℓ_t must be corrected for this additional driving force.

2.2.1.6 Conclusion - Hydrodynamic Model

The overall driving gravity pressure difference is, therefore,

$$\Delta P_g = H_t + H_{cd} - (H_e + H_a + H_{cu}) \qquad (\text{dynes/cm}^2) \qquad (2.2\text{-}25)$$

and the sum of the frictional and acceleration pressure difference terms is

$$\Delta P_a + \Delta P_f = R_{ef} + R_{ea} + R_{af} + R_{asf} + R_{asc} + R_{cuf} + R_{cua} + R_{cue} + R_{cdc} + R_{cda} + R_{cdf} + R_{tc} + R_{tf} + R_{te} \quad (\text{dynes/cm}^2) \qquad (2.2\text{-}26)$$

A hydrodynamically balanced mass flux results in the equality

$$\Delta P_g = \Delta P_a + \Delta P_f \qquad (2.2\text{-}27)$$

and this condition signifies a valid heat pipe operating point.

2.2.2 Parametric Analysis

The cocurrent flow heat pipe model developed in the previous sections has two parameters, X_1 and X_2, which must be selected on an empirical basis. The parameter X_1 is the quality of the two-phase mixture exiting the evaporator while X_2 is the quality of the two-phase mixture entering the condenser. On a theoretical basis, X_2 must equal X_1, but, in fact, it is desirable to maintain X_2 independently adjustable to correct for leakage across the condenser separator plate. This plate cannot be expected to hermetically seal the opposing half-sections and, in fact, experiments in which a glass heat pipe section was used showed that considerable leakage does occur. These experiments also showed that the quality of the mixture exiting the evaporator approaches 90-100% near burnout, so that if burnout points are the only operating points of interest, the exit quality X_1 does not have to be substantially varied.

Figure 2.2.3 presents predicted transport capacities at 25°C for the "Phase 7" heat pipe described in Section 3 using R-11 as working fluid and $X_1 = 0.9$ and $X_2 = +0.67$. The capacity is shown as a function of the ratio of the condensate return tube hydraulic radius $R_{h\ell}$ to the hydraulic radius of the evaporator two-phase boiling section, R_{hv}. The figure shows that the optimum ratio of $R_{h\ell}$ to R_{hv} is not a function of tilt angle and is approximately $R_{h\ell}/R_{hv} = 0.65$.

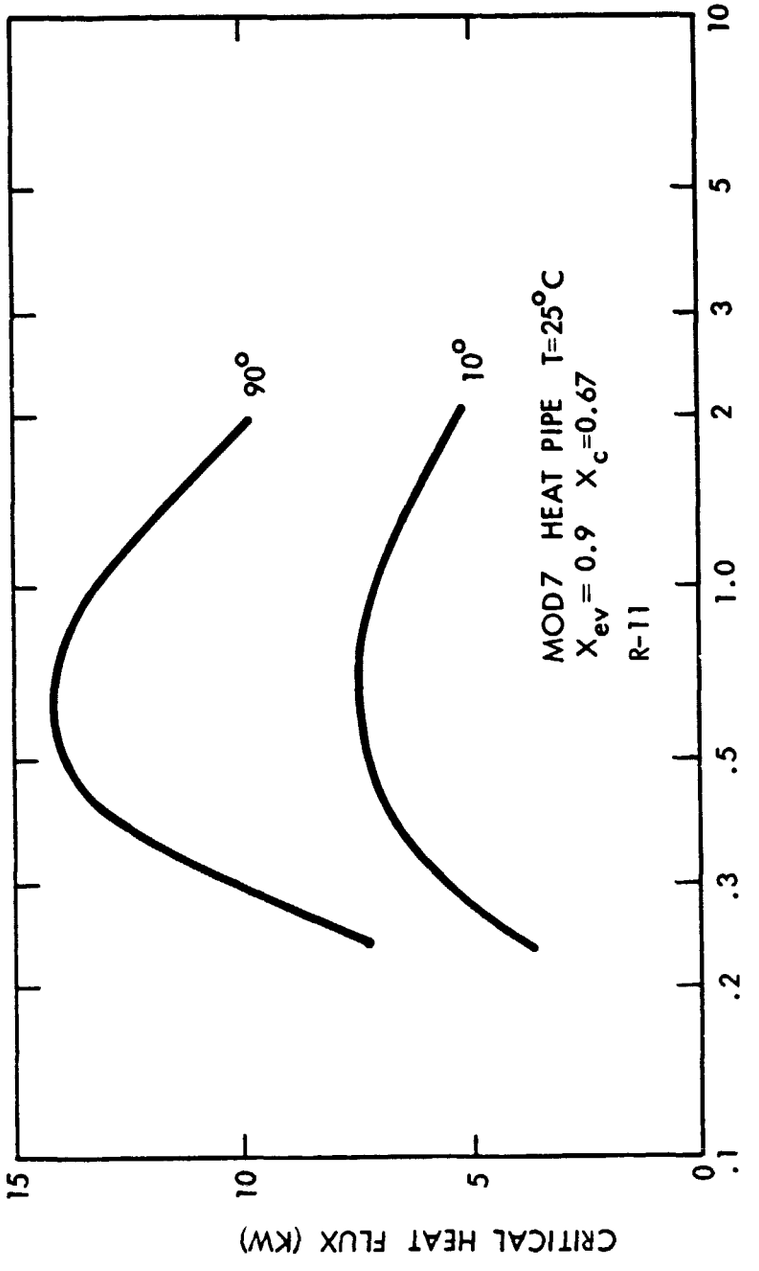

FIGURE 2.2.3. CALCULATED TRANSPORT CAPACITY FOR PHASE 7 COCURRENT FLOW HEAT PIPE AT 10 AND 90° REFLUX TILTS AS A FUNCTION OF THE LIQUID/VAPOR HYDRAULIC RADIUS RATIO FOR THE EVAPORATOR SECTION.

This optimum ratio will change with changes in fluid properties and lengths of each heat pipe section, but it can be expected that in most cases, the ratio will be less than or equal to 1.0.

Figures 2.2.4 and 2.2.5 show the influence of the qualities X_1 and X_2 on predicted performance. Also shown in these figures are the predicted performances of bare tube thermosyphons of equal diameter. The predicted critical heat fluxes at the best estimate values of evaporator exit and condenser inlet qualities (X_1 = 0.9, X_2 = 0.67) are bounded within approximately 20% by the conservative estimates of X_1 = 0.95, X_2 = 0.9, and X_1 = 0.8, X_2 = 0.5. It can, therefore, be concluded that the effects of X_1 and X_2 are measurable, but not dramatically so. It should also be noted that the effects of vapor qualities on predicted critical heat flux are much less pronounced at lower temperatures (lower saturation pressures).

2.2.3 Comparison of Fluids for Heat Pipe Applications

Table 2.2.1 presents the predicted critical heat fluxes for various fluids using either a conventional open-core reflux heat pipe or a cocurrent flow reflux pipe. In 11 cases a vertical, 2.54 cm I.D. tube was assumed. For the cocurrent calculations, a separator design, referred to as Phase 10 in Section 3 of this report, was assumed. Operating temperatures were selected such that the saturation pressure of the fluid was 2 atm (2.03×10^6 dynes/cm^2). By performing all the calculations at the same saturation pressure, the vapor energy density (vapor density times heat of vaporization) was approximated equal for all the fluids examined.

The fluids examined covered a range from cryogenic liquids to molten metals and included common refrigerants, heat transfer fluids, hydrocarbons, and water. Additional fluids of interest may be found in a report by Saaski and Owzarski.[32]

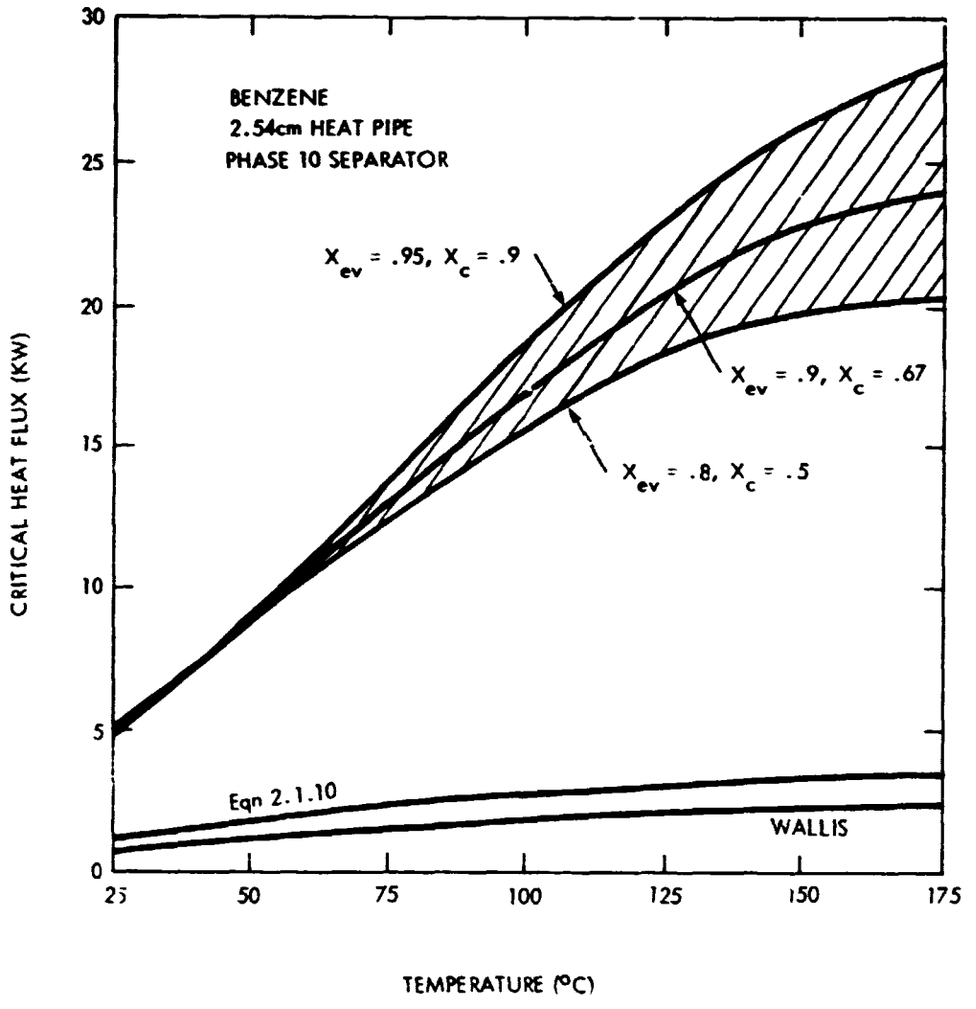

FIGURE 2.2.4. THE EFFECT OF EVAPORATOR EXIT QUALITY, X_{ev}, AND CONDENSER ENTRANCE QUALITY, X_c, ON THE PERFORMANCE OF A COCURRENT FLOW HEAT PIPE CHARGED WITH BENZENE.

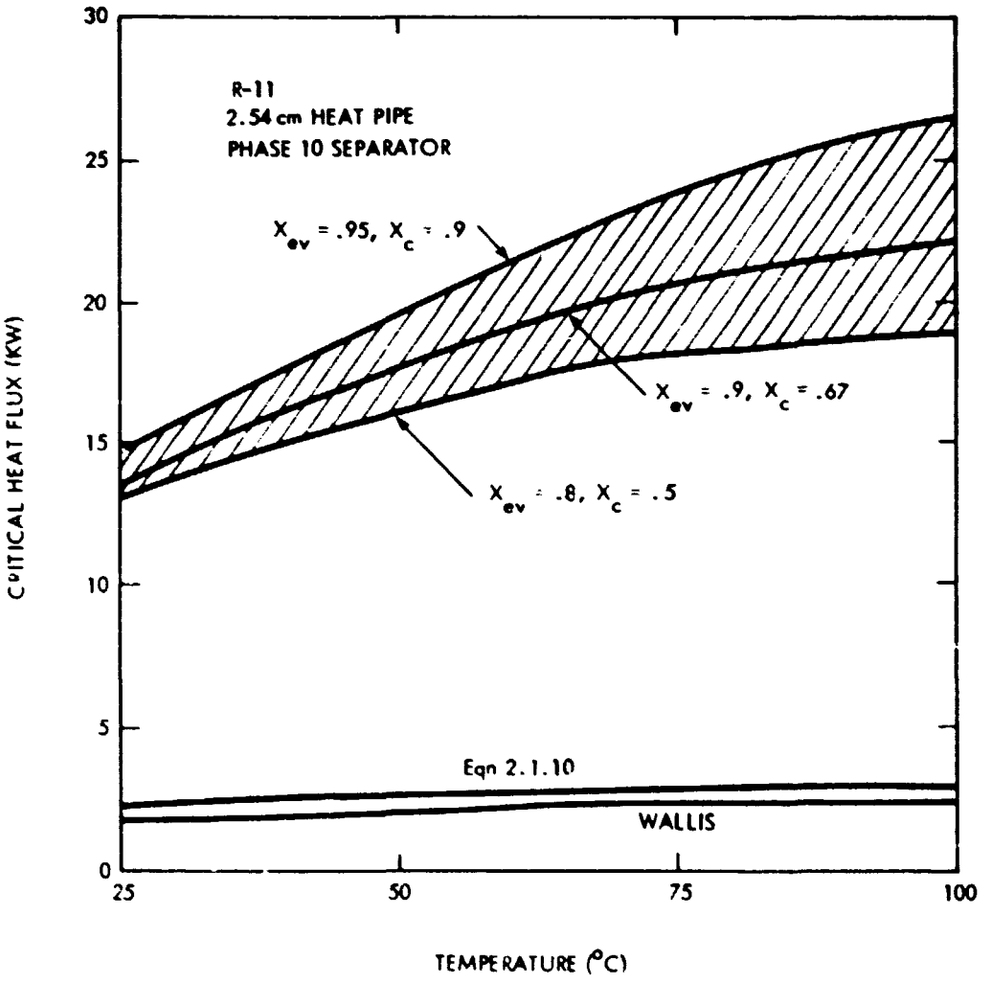

FIGURE 2.2.5. THE EFFECT OF EVAPORATOR EXIT QUALITY, X_{ev}, AND CONDENSER ENTRANCE QUALITY, X_c, ON THE PERFORMANCE OF A COCURRENT FLOW HEAT PIPE CHARTED WITH R-11.

TABLE 2.2.1. CRITICAL HEAT FLUX FOR VARIOUS FLUIDS AT P_{SAT} = 2 ATM

Liquid	Temperature (°C)	Bo	$\rho_v h_{fg}$ $\left(\frac{\text{Joules}}{\text{gm}}\right)$	$\rho_\ell h_{fg}$ $\left(\frac{\text{Joules}}{\text{gm}}\right)$	Wallis* Eqn. 2.1-1 (Watts)	Eqn. 2.1-10* (Watts)	Cocurrent* Model (Watts)
N_2	-190	26.4	2.32	148	1336	1,131	14,124
Ethane	-75	15.4	1.81	247	1678	1,517	15,762
NH_3	-20	11.6	2.10	882	3836	3,548	32,360
R-11	45	23.9	2.20	297	2025	1,736	20,370
Benzene	105	16.5	1.95	297	1929	1,734	17,618
H_2O	120	10.7	2.42	1952	6480	6,041	52,349
$TiCl_4$	165	22.8	1.90	257	1753	1,514	17,045
Dowtherm-E	210	21.1	2.09	278	1904	1,663	18,221
Dowtherm-A	290	19.7	2.02	232	1680	1,478	16,124
Se	750	21.9	2.10	3533	8568	7,446	66,606
K	840	8.2	1.96	1233	4532	4,286	34,884

-Eqns. 2.1-1 and 2.1-10 are based on 2.54 cm bare tube.

-Cocurrent model is based on 2.54 cm I.D. with Phase 10 separator

*Values expressed to units digit for comparison only.

As can be seen from the table, liquid energy density, liquid density times heat of vaporization, is a dominant factor in determining the performance of both the bare tube and the cocurrent heat pipes. This is to be expected since at a constant vapor energy density, the capacity of all these devices is limited by the rate at which liquid can be returned to the evaporator. Higher liquid densities provide greater driving forces to return the liquid and higher heats of vaporization yield larger heat transfer rates per volume of liquid evaporated. It is interesting to note that for the cocurrent heat pipe with the Phase 10 separator, the critical heat flux correlates well with the square root of the liquid energy density, $[Q(kW) \approx 34.4 \sqrt{\rho_\ell h_{fg}\ (kJ/gm)}]$.

Titanium tetrachloride is of particular interest in that it is thermally stable and relatively noncorrosive in a temperature range of interest for commercial heat recovery applications. Tests at Sigma Research, Inc. have shown over 20,000 hours of operation of $TiCl_4$ in heat pipes made of carbon steel at temperatures in the range of 150-170°C.

Of the non-liquid metals, water shows the highest heat flux capability for both open core heat pipes and cocurrent flow heat pipes, with calculated transport capacities respectively of 6500-11,000 watts and 52,000 watts. The poorest fluid is liquid nitrogen at 1300-1600 watts and 14,000 watts capacity, respectively, for conventional and cocurrent flow 2.54 cm diameter heat pipes. Most refrigerants and heat transfer fluids indicate transport capacities of 1100-2500 watts for a conventional reflux heat pipe, and 15,000 to 20,000 watts in a cocurrent heat pipe. In general, it can be concluded that a factor of 5 to 10 improvement in capacity is obtained by eliminating countercurrent vapor/liquid shear.

3.0 EXPERIMENTAL TESTS

3.1 Test Apparatus

Heat pipes developed for this project were tested in one of two test stands constructed for this purpose. These test stands consisted of a heat source, cooling water supply, means for adjusting the tilt of the heat pipe, and appropriately placed thermocouples. The first test stand developed used low-pressure steam to heat the evaporator. In later tests, a direct coupled water loop was used.

3.1.1 Low-Pressure Steam System

In this system, shown in Figure 3.1.1, heat was transferred to the heat pipe using a water boiler and steam jacket. This method of heating approximated a constant-temperature boundary condition and allowed the heat pipe to operate in a partially burned out evaporator condition. A previous test system using a resistance-heated evaporator was discarded because of hot spot problems resulting from local dry-out, and because a constant flux boundary condition does not truly reflect the performance of a heat recovery heat pipe. In a heat recovery system, the heat pipe wall does not rise indefinitely in temperature if a partial dry-out occurs because (1) the gas stream-to-fin temperature differential falls, reducing local heat input; (2) the heat pipe wall and exterior fins conduct heat circumferentially to areas that are wetted; and (3) the available driving temperature differential may not be particularly large in many applications. Furthermore, extensive reflux heat pipe test programs in the USSR[17] have used resistance heating and the adverse effects of tilt on capacity discussed in these reports do not coincide with the observed behavior of air-to-air heat recovery heat pipes produced by U. S. manufacturers,[12] while the data collected in this program do agree with the latter report in terms of tilt effects on transport capacity. However, it should be recognized that a constant-temperature boundary condition is still only an approximation of diverse possible operating conditions, and some differences in performance can be expected between this simulation and the actual article near burnout.

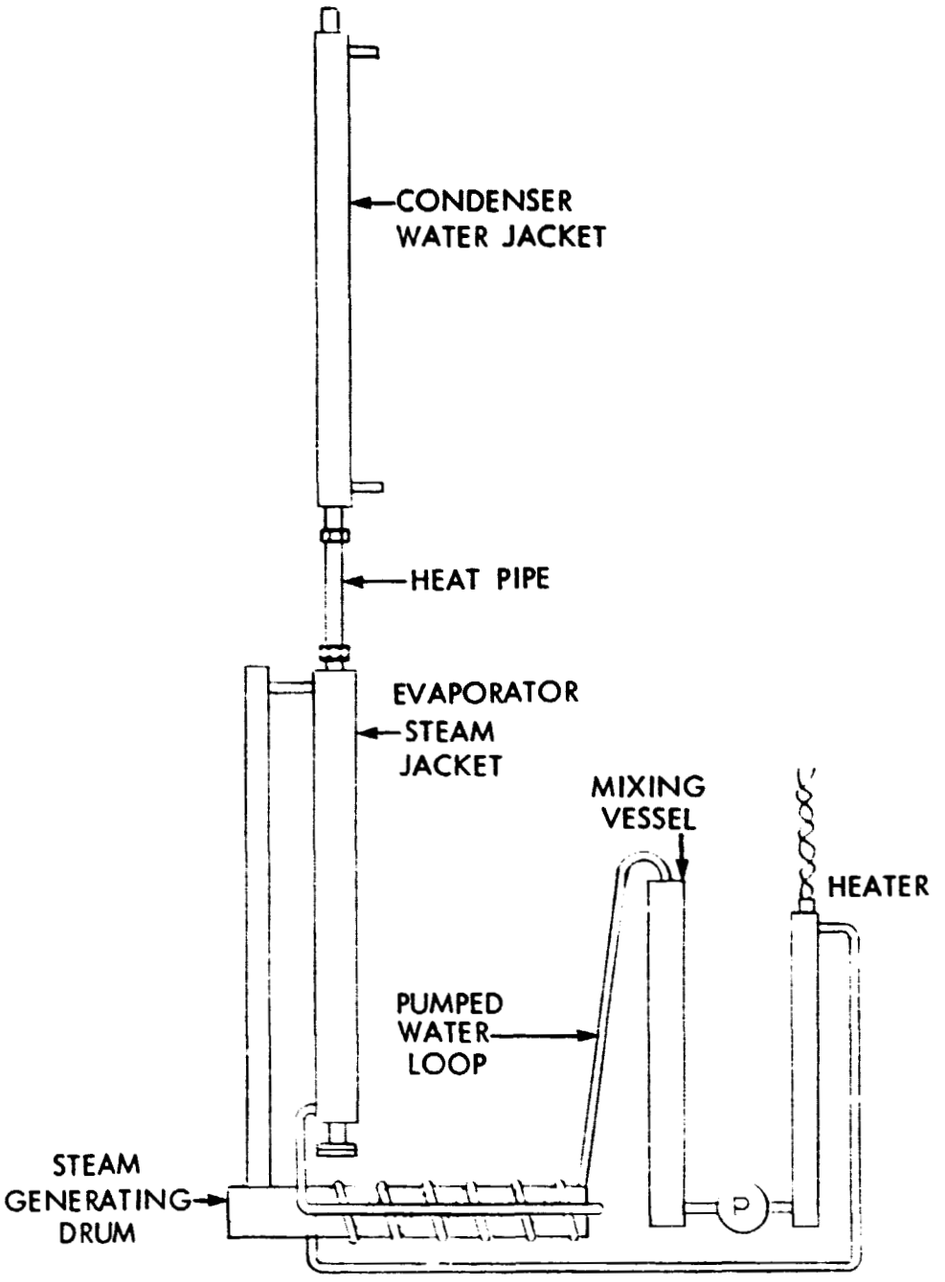

FIGURE 3.1.1. INITIAL TEST SET-UP FOR REFLUX HEAT PIPE TESTS.

Heat input to the heat pipe was measured in two ways. The steam boiler supplying the heat pipe was heated by a water loop, and heat input to the boiler by this liquid loop was measured by calorimetric means ($\dot{m}C_p\Delta T$), while the heat pipe condenser was cooled by an annular water jacket that also could be used as a flow calorimeter at higher power levels. Both sets of thermocouples were selected on the basis of identical readings at ice bath temperature and 100°C, when used in conjunction with a 0.1°C resolution Doric DS-350 digital thermocouple readout. The Chromel-Alumel thermocouples were directly soldered to the inlet and outlet water connections and were well insulated.

External heat loss from the insulated steam jacket was measured with the heat pipe in a dry condition, and was found to be described by a constant conductance of 1.41 W/°C. Hence, at a typical water temperature of 65°C, about 63 watts were lost to a 20°C ambient.

Prior to testing, the heat pipe was mounted in a large rigid frame and adjusted to a vertical orientation using a 61 cm long spirit level. Other angles were calculated by direct measurement of differential height from end-to-end of the heat pipe.

3.1.2 Water Loop

In order to operate at the higher powers necessary to test the high-capacity heat pipes developed during this program, a water loop heating system was constructed. This loop is shown schematically in Figure 3.1.2. Also shown in this drawing are the locations of the thermocouples used to measure the performance of the heat pipe. The specific thermocouple numbers given in Figure 3.1.2 are those used in the Mod-6 through Mod-10 tests; other numbering schemes were used in earlier tests.

A mixing vessel, with a volume of approximately two liters, was used to provide a free surface. This ensured that the system could not become pressurized. The vessel drained into the inlet of a small pump. The capacity of the pump was approximately 350 to 425 cubic centimeters per second, depending on the

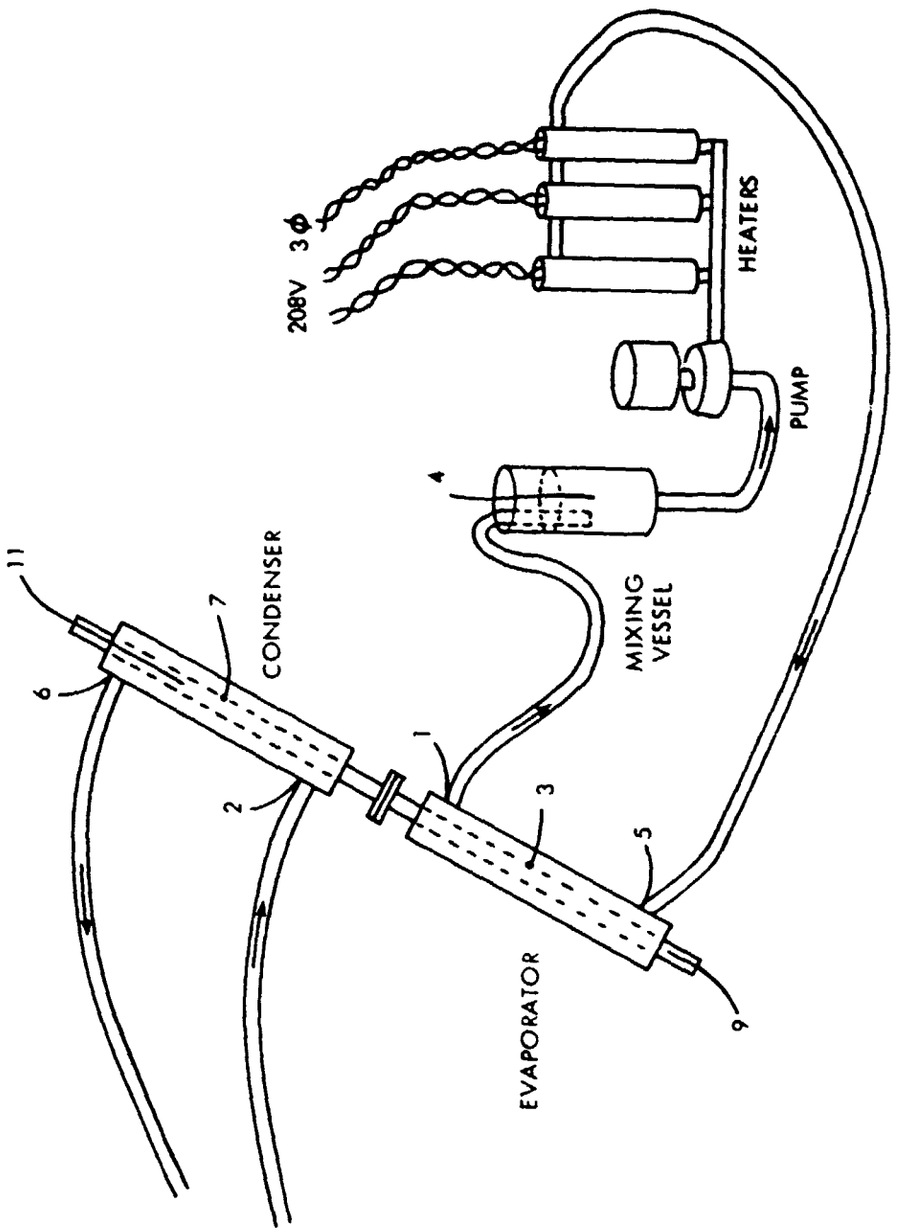

FIGURE 3.1.2. HIGH POWER PUMPED WATER LOOP FOR REFLUX HEAT PIPE TESTS.

piping arrangement used for the test. Measurements showed the flow rate, for any particular arrangement, to be constant over the temperature ranges experienced during operation (25-100°C).

The discharge of the pump was connected to a heater manifold. This manifold initially contained approximately 3000 watts of electrical heaters. As heat pipe capacities increased, additional elements were added to provide 6000, 12,000 and finally 15,000 watts of heat input. The heating elements used were commercially available units for hot water heating.

The mixing vessel, pump, and heater manifold were mounted on a chassis along with the necessary electrical controls. This assembly was connected to the evaporator heating jacket with foam-insulated high-pressure high-temperature hose. Overall heat losses from the total system ranged from 250 to 1500 watts, depending on the operating temperature.

3.1.3 Heat Pipe Description - Definition of Burnout

The heat pipes tested in this program (Figure 3.1.3 and 3.1.4) used three different evaporative surfaces: a single layer of 200-mesh stainless screen, a proprietary boiling surface--High Flux which is manufactured by Linde Division of Union Carbide, and a bare tube surface. The condenser surface in all cases was bare, as-received Type K copper tube.

Most of the open tube thermosyphon tests described in Section 3.2.1 were performed with a bare evaporator wall of Type K copper. Although some of the data for benzene and R-11 were taken with the previously mentioned 200-mesh screen surface, these data have not been separately identified because no significant effect of the screen on critical axial heat flux was identified. Subsequent tests performed on the cocurrent flow heat pipe used either a bare evaporator tube wall or the Linde High Flux surface. The particular evaporative surface used in each test

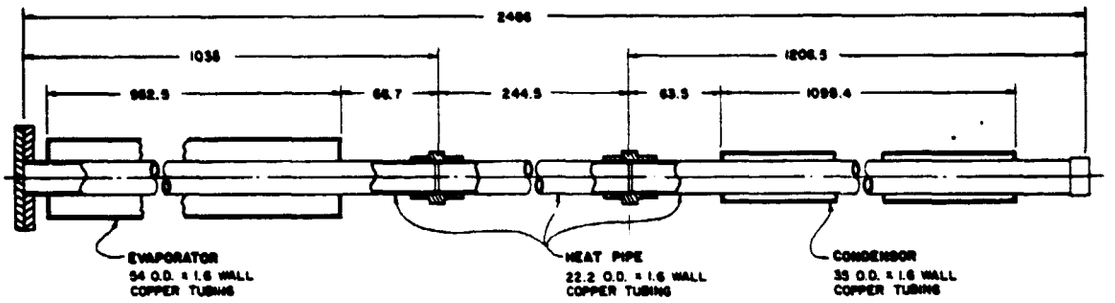

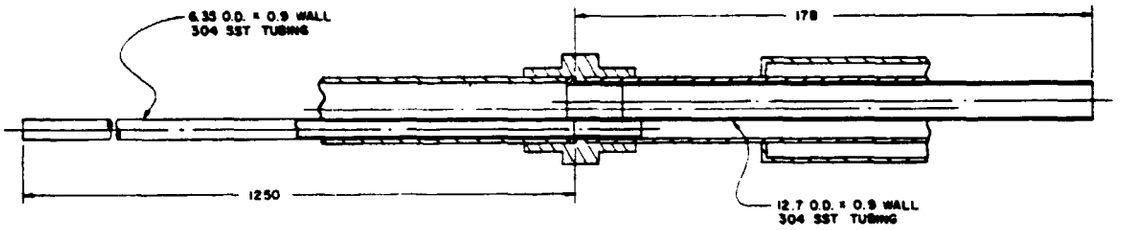

PHASE I SEPARATOR

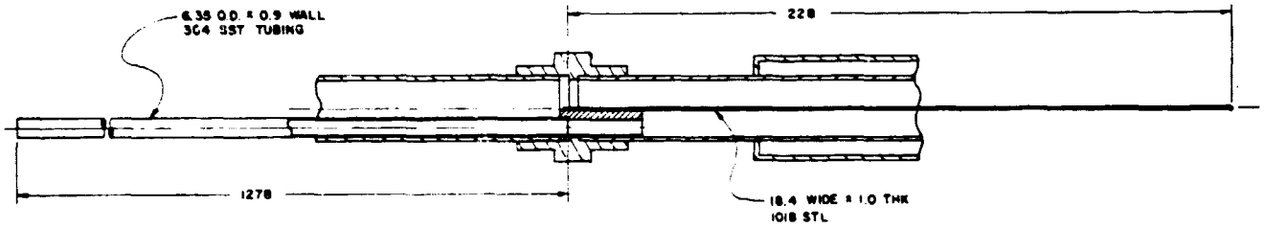

PHASE II SEPARATOR

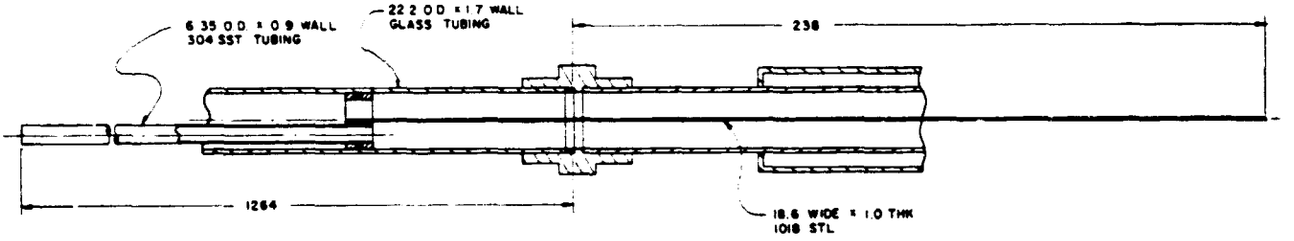

PHASE III SEPARATOR

FIGURE 3.1.3. HEAT PIPE AND SEPARATORS USED IN OPEN-CORE TESTS AND PHASE 1 THROUGH PHASE 3 TEST SEQUENCES.

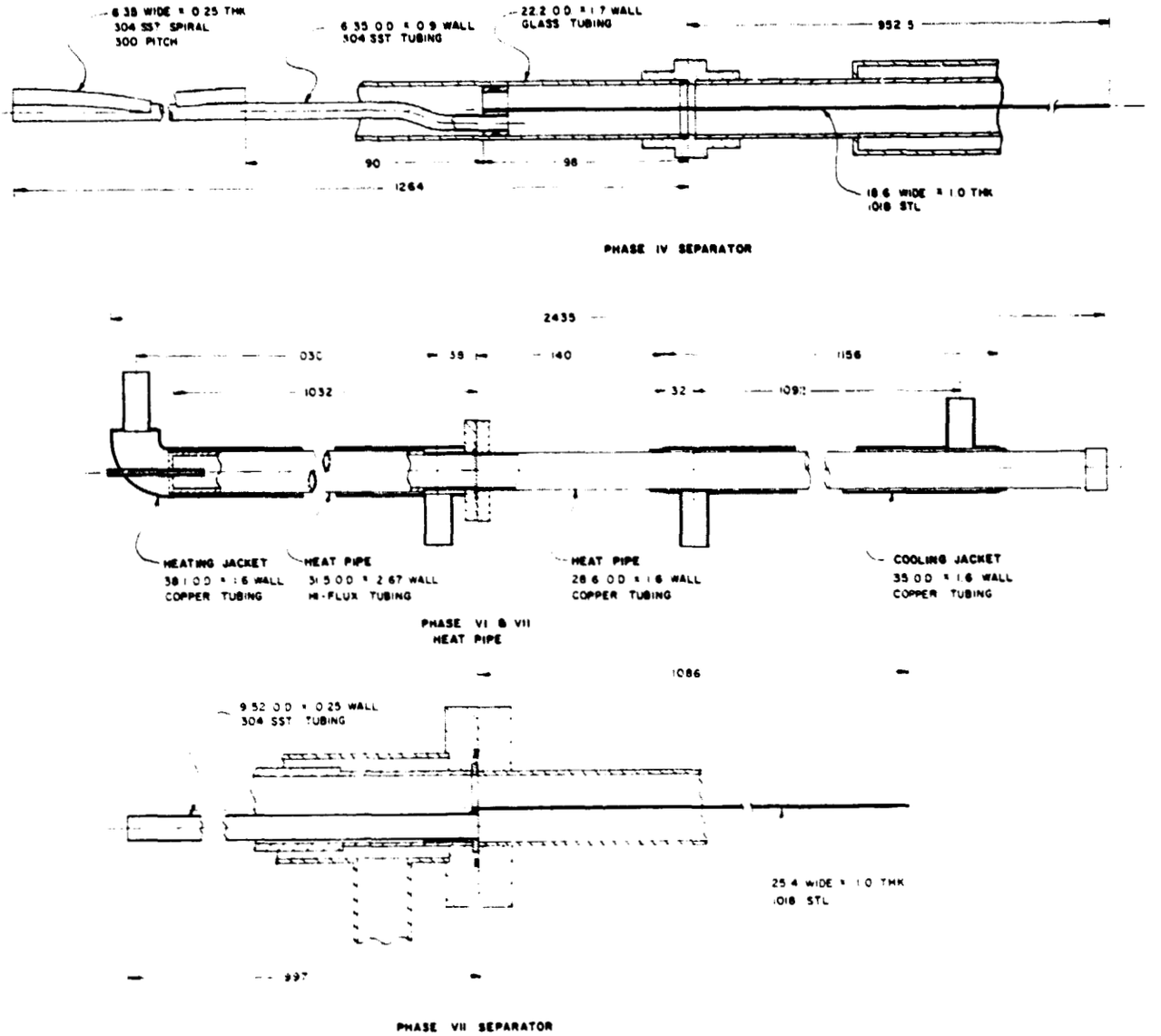

FIGURE 3.1.4. PHASE 4/5 SEPARATOR AND HEAT PIPE/SEPARATOR ASSEMBLIES USED IN TEST PHASES 6 THROUGH 10.

sequence is identified in Section 3.2.2. The Linde High Flux surface was a sintered layer of copper on a substrate of cupronickel.

In all tests, the liquid charge used was one which would fill approximately 60% of the evaporator under static saturated conditions at 25°C. Where relevant, actual gram loadings are called out in subsequent sections.

Heat pipe "burnout" was defined as follows. It was observed in all cases that a plot of the overall heat pipe conductance versus heat flux showed a steadily increasing value of conductance with heat throughput until burnout was imminent. Near burnout, the heat pipe conductance would stabilize and then begin to fall, in many cases, very sharply. For all test runs, burnout was identified as the heat flux at which the overall conductance peaked. This means that at "burnout" the heat pipe was still functional; in many runs the difference between this burnout flux and a thermal runaway heat flux was quite small--in other cases, the flux at thermal runaway was as much as 50% greater.

The heat flux at peak conductance was defined as burnout because it was felt that the subsequent reduction in conductance with heat input was the most clear signal of a fundamental and degrading change in heat pipe operation.

3.2 Experimental Performance

An extensive series of tests has been performed to provide an experimental basis for the heat pipe model developed in this project. These tests also provided a comparison between open core heat pipes and the enhanced capacity cocurrent heat pipes which were developed as part of this project.

3.2.1 Open Core Heat Pipes

Figure 3.2.1 is a plot of critical heat flux versus tilt from horizontal, for four different fluids, in a 1.91 cm I.D. bare tube heat pipe. Table 3.2.1 presents physical properties of the test fluids.

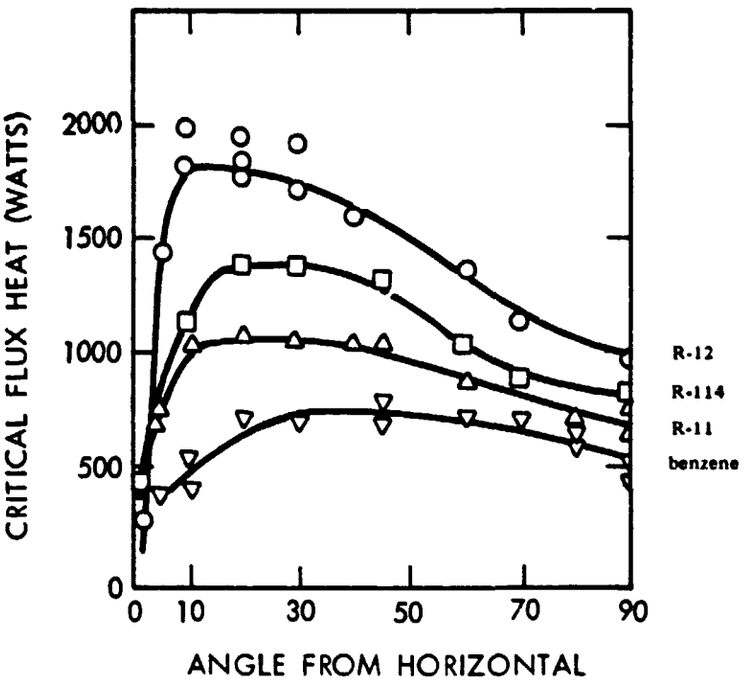

(3.2.1)

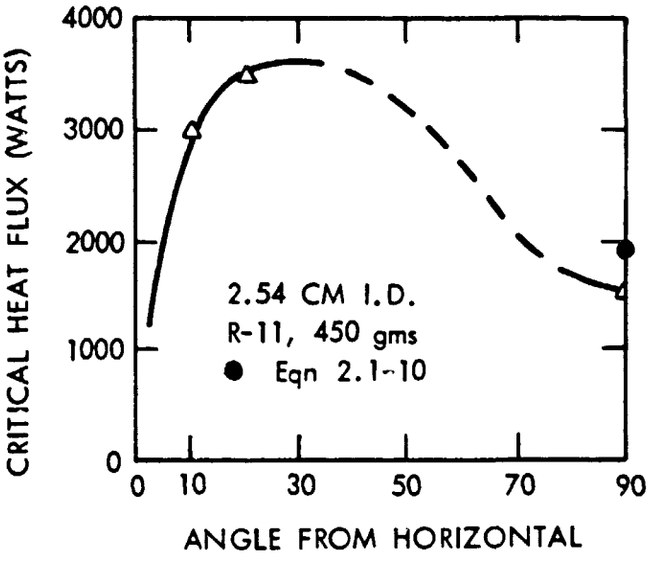

(3.2.2)

CRITICAL AXIAL HEAT FLUXES FOR A 1.91 CM I.D. REFLUX HEAT PIPE WITH FOUR DIFFERENT WORKING FLUIDS (FIGURE 3.2.1) AND CRITICAL AXIAL HEAT FLUX FOR A 2.54 CM I.D. REFLUX HEAT PIPE CHARGED WITH R-11 (FIGURE 3.2.2).

P 2.1-7

$$B_o = \sqrt{\frac{\nu^2 g(\rho_\ell - \rho_v)}{\sigma}}$$

buoyancy effects $= D g (\rho_\ell - \rho_v)$

capillary $= \sigma/D$

Note entrainment normally depends on Weber no.

$$W = \frac{\rho_v v^2/g_c}{(\sigma/d)} \quad \begin{array}{l}\text{inertia forces} \\ \text{surface tension}\end{array}$$

For
$$Q = \rho A v h_{fg} = \rho_v u_v h_{fg} \frac{\pi}{4} d^2$$

$$Q^2 = (\rho_v u_v^2) \rho_v h_{fg}^2 \left(\frac{\pi}{4}\right)^2 d^4$$

or
$$Q^2 = 2 g_c W \frac{\sigma}{d} \rho_v h_{fg}^2 \left(\frac{\pi}{4}\right)^2 d^4$$

or
$$Q = \frac{\pi}{4}\sqrt{2}\left[W \sigma \rho_v h_{fg}^2 d^3\right]^{1/2}$$

∴ One might expect

$$Q_{\substack{\text{critical} \\ \text{entrainment}}} \sim \sqrt{\sigma \rho_v h_{fg}^2}$$

TABLE 3.2.1. TEST FLUID PHYSICAL PROPERTIES

Working Fluid/ Temperature (1)	Liquid Density, ρ_ℓ (g/cm^3)	Vapor Density, ρ_v (g/cm^3)	Bond Number (2)	Vapor Energy Density, $\rho_v h_{fg}$ (W/cm^3)
Benzene/25°C	0.868	0.000505	10.5	0.218
R-11/30°C	1.46	0.00717	17.2	1.28
R-114/35°C	1.43	0.0213	21.4	2.64
R-12/ 40°C	1.255	0.0552	24.5	7.09

(1) Temperature at peak heat flux used for property evaluations.

(2) For a diameter of 1.905 cm.

The tests clearly show four qualitative features of reflux heat pipe operation and the effect of fluid selection: (1) a high latent heat and gas phase density result in greater transport capacity at all tilts; (2) heat flux versus tilt behavior is very similar for all fluids tested, indicating a common physical mechanism of burnout; (3) heat fluxes at near-horizontal are very low; and (4) the absolute maximum axial flux occurs at a reflux angle less than 90°.

Aside from the obvious beneficial effects of reducing vapor/liquid shear through an increased vapor phase energy density ($\rho_g h_{fg}$), it is interesting to note the strong positive influence of liquid/vapor stratification which occurs when the heat pipe is not in a vertical orientation. The condensate stream or puddle formed by tilting shields more of the condensate from vapor shear by improving the ratio of shear area to condensate flow cross-sectional area.

The Bond numbers of the fluids tested range from about 10 to 25. It might be expected that fluids with a large Bond number would have higher peak heat fluxes because of the weakness of surface tension forces relative to gravity forces, i.e., high Bond number fluids would have puddles with a minimum vapor shear area. The peak heat fluxes of each fluid do, in fact, fall in the same order as their Bond numbers, and the reflux angle at the absolute maximum heat

flux decreases with increasing Bond number. Benzene, with a Bond number of about 10, has a maximum axial flux of about 750 watts at a 30 to 50° tilt, while R-12, with a Bond number of 24.5, has a maximum axial flux of about 1800 watts at a tilt angle of 10 to 20°. In all cases, the axial flux at a 90° tilt is substantially less than the flux at the optimum angle, that is, as much as one-third to one-half lower than the flux at the optimum tilt. There are no analytical or empirical models in the literature that predict this behavior.

The peak heat flux in a vertical orientation has been studied in some detail, as discussed in Section 2.1. Figure 2.1.3 compares the data shown in Figure 3.2.1 with the model of Tien and Chung, and the recommended correlation, equation (2.1-10), given in Section 2. In general, the data fall within 50% of the Tien and Chung model, and is in good agreement with equation (2.1-10) if C_w is in the range $0.725 \leq C_w \leq 0.95$.

Figure 3.2.2 gives the experimental results for critical heat flux for R-11 in a 2.54 cm I.D. heat pipe incorporating the High Flux evaporative surface. Also shown in this figure is the value for a 90° tilt predicted by equation (2.1-10).

3.2.2 Enhanced Performance Heat Pipes

Capacity Enhancement

It is apparent that one of the primary factors limiting peak heat transfer in a reflux heat pipe is countercurrent vapor/liquid shear. The shear process and related phenomena of wave action and droplet entrainment serve to starve the evaporator of liquid and cause burnout. Hence, the primary goal must be to develop a means of counteracting the interfacial shear or actually using it to enhance performance.

The most obvious means of enhancing capacity is to separate the liquid and vapor flows so that the destructive mechanisms related to shear are eliminated. For nominally horizontal reflux heat pipes, this can be done by placing a smaller diameter tube in the heat pipe and filling the heat pipe to a level such that the condenser end of the heat pipe is flooded, thereby providing a fluid return to the extreme evaporator end.[12] A second technique that has been used on vertical reflux liquid metal heat pipes is to provide axial flow channels or "gutters" for condensate to minimize the vapor/liquid contact area and thereby limit shear.[32] Both of these techniques will provide substantial capacity improvements, and the secondary tube approach is reasonably cost-effective and immune to boiling within the condensate return. The axial flow channel is satisfactory for liquid-metal heat pipes but could pose problems for organic heat recovery heat pipes where the wall superheat is greater, the tendency towards nucleate boiling is more pronounced, and liquid surface tensions lower. Section 3.2 describes the class of flow separator approaches tested in this program. These tests resulted in a separator optimized for organic and fluorocarbon working fluid heat pipes.

A summary of test results for various vapor-liquid separators, along with data for pipes without separators, is given in Table 3.2.2.

General Description of Test Phases

All tests listed in the table were performed with R-11 working fluid, and are identified by axial transport capacity and the corresponding vapor core temperature. Test sequences 1 through 5 were performed with a 1.905 cm I.D. bare evaporator surface and a relatively small 0.45 cm I.D. condensate return tube. The Phase 1-3 tests used a relatively short separator plate that penetrated only a short distance into the condenser zone. These separator plates increased capacity at low tilt angles by about a factor of two relative to an open-sectioned heat pipe, but had no substantive effect on vertical reflux performance.

TABLE 3.2.2. DATA SUMMARY FOR CONVENTIONAL AND HIGH-PERFORM
REFLUX HEAT PIPE TESTS USING R-11[1]

Tilt Angle (deg)	Screened Evaporator (W/°C)	Base Tube (W/°C)	Phase 1 Tests (W/°C)	Phase 2 Tests (W/°C)	Phase 3 Tests (W/°C)	Phase 4 Tests (W/°C)	Phase 5 Tests (W/°C)	Phase 6[2] Tests (W/°C)	Pha Te (W
0		<200/19							
5		610/21[3]	>800/34		1210/36	970/37	No		~4
10	905/27	990/28	1100/31	1560/43	1880/47.5	1730/48	change	3000/40	~6
20	>940/27	1030/27	1290/36	>1980/50	2510/56	2400/54	from	3500/38	
30	1075/30	1000/30	1870/41		>2790/61	2840/58	Phase		
40	>1035/30				>2720		4		
45		1000/30	1710/41	2170/48		>2980/57			>10,2
50	1020/31.7				>2720				
60	1050/30.5	840/28	1760/42		2710/58	>2980/57			
70	790/27	831/24	1760/41		2440/52	>2980/56			
80	800/29	660/22	1450/40						
90	810/26	750/23	1340/38	1230/30	1250/34	>3030/57		1550/32	>10,2

[1]Initial liquid load = 240 g of R-11.

[2]Initial liquid load = 450 g of R-11.

[3]4.3° tilt.

FOLDOUT FRAME

MARY FOR CONVENTIONAL AND HIGH-PERFORMANCE
EAT PIPE TESTS USING R-11[1]

Phase 4 Tests (W/°C)	Phase 5 Tests (W/°C)	Phase 6[2] Tests (W/°C)	Phase 7[2] Tests (W/°C)	Phase 8[2] Tests (W/°C)	Phase 9[2] Tests (W/°C)	Phase 10[2] Tests (W/°C)
970/37	No		∿4000/60	∿3500/50	∿5600/75	5500/75
1730/48	change	3000/40	∿6500/72	∿7000/70	>7300/82	7100/81
2400/54	from	3500/38				>8500/81
2840/58	Phase					>14,000/74
	4					>9800/80
>2980/57			>10,200/78			>13,800/70
>2980/57						
>2980/56						>15,200/70
>3030/57		1550/32	>10,200/76	>10,200/79		>14,200/67

FOLDOUT FRAME 2

TABLE 3.2.2. CONTINUED

Identification of Tests

Base Tube:	Bare, 1.9 cm inside diameter heat pipe. Figure 3.1.3.
Screened Evaporator:	1.9 cm diameter with 200-mesh screen lining in evaporator.
Phase 1:	1.9 cm heat pipe with 17.9 cm long separator tube and 0.45 cm I.D. return tube. Figure 3.1.3.
Phase 2:	1.9 cm heat pipe with 22.8 cm long separator plate and 0.45 cm I.D. return tube. Figure 3.1.3.
Phase 3:	1.9 cm heat pipe with transparent adiabatic section.
Phase 4:	1.9 cm heat pipe with transparent adiabatic section; 105 cm long separator plate and 0.45 cm I.D. return tube. Figure 3.2.4. (Phase 4 modification is shown with Phase 5 evaporator spiral. Phase 4 condensate tube is the same as that used in Phase 4, minus the spiral.) Figure 3.1.3.
Phase 5:	1.9 cm heat pipe with transparent adiabatic section, 105 cm long separator plate and spiral insert in the evaporator section. Phase 4 modification, Figure 3.1.4.
Phase 6:	2.54 cm heat pipe with Linde High Flux* evaporator surface and no separator. Figure 3.1.4.
Phase 7:	2.54 cm heat pipe with High Flux evaporator, 108.6 cm long separator plate and 0.9 cm I.D. return tube. Figure 3.1.4.
Phase 8:	2.54 cm heat pipe with High Flux evaporator, 108.6 cm long separator, oriented vertically and 0.9 cm I.D. return tube.
Phase 9:	2.54 cm heat pipe with High Flux evaporator, 108.6 cm long separator and perforated 0.9 cm I.D. return tube.
Phase 10:	2.54 cm heat pipe with High Flux evaporator, 108.6 cm long separator and 1.2 cm I.D. return tube. Figure 3.1.4.

* Commercial designation of proprietary porous boiling surface manufactured by Linde Division of Union Carbide Corporation.

FIGURE 3.2.3

Separator test sequence No. 3, 50° tilt, 2400 watts, 1/500-second exposure time. Condensate capture pocket on right side of separator plate is full of liquid, and vapor-liquid flow in heat pipe core is a mixture of annular and puddle flow. Heat pipe core flow patterns at 30 and 40° tilts look similar to the flow pattern in this photograph.

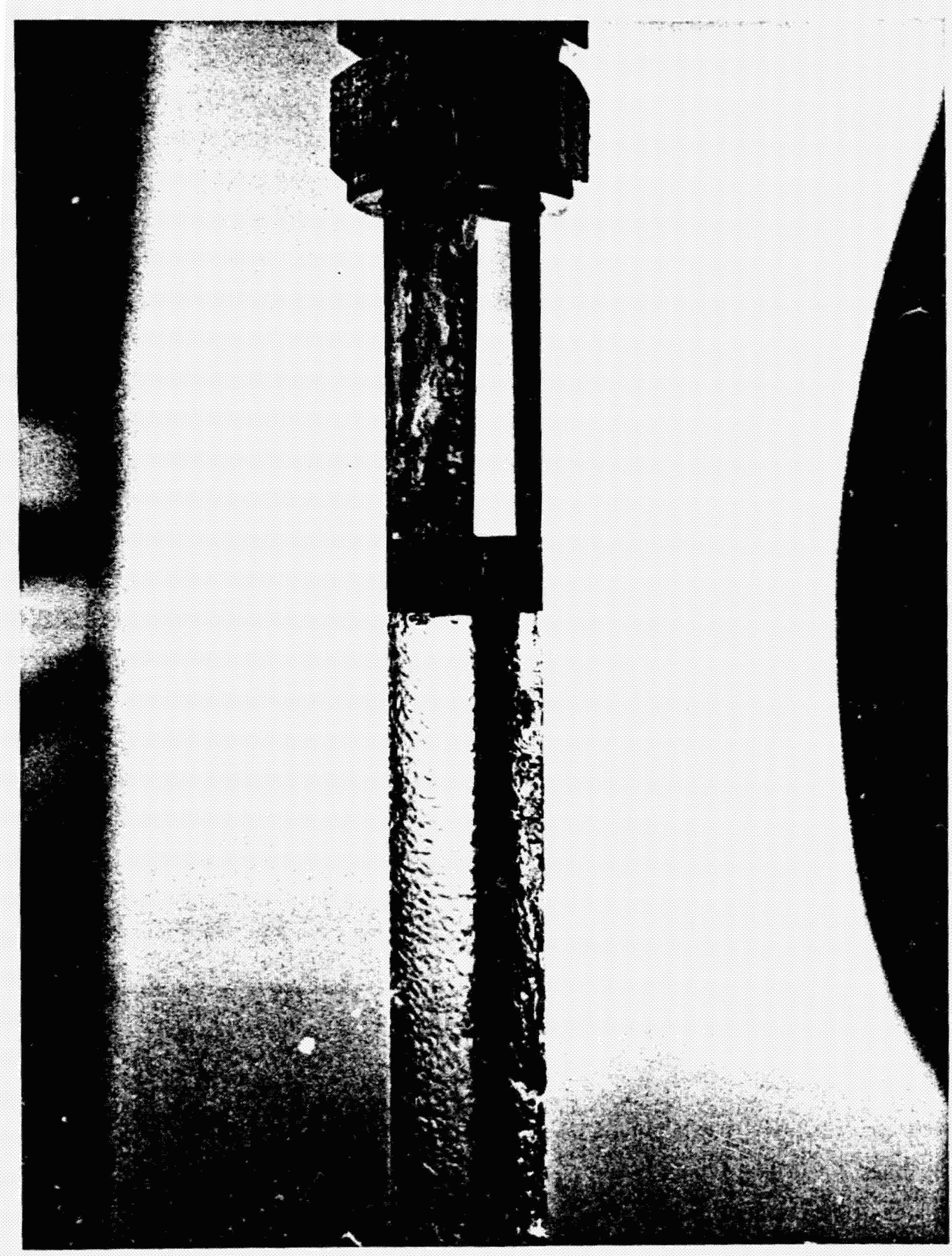

The Phase 3-5 test sequences were performed with a glass adiabatic section so as to observe heat pipe dynamics. Figure 3.2.3 is a representative photograph of the Phase 7 heat pipe at a flux of about 2500 watts.

In Phase 4, the separator plate length was increased so that almost the entire condenser was split into halves. This permutation had a dramatic effect on vertical operation. With the long separator plate, vertical reflux heat pipe capacity exceeded the capabilities of the pumped water loop, providing a factor of 2.5 gain over the earlier open tube tests. The longer separator plate reduced transport capacity at tilt angles less than or equal to 30° by about 5 to 20%. Overall, the gains associated with the long separator plate far outweighed the small reduction in capacity at low tilt angles. In Phase 5, a spiral insert was used in the evaporator in an attempt to improve evaporative heat transfer coefficients. The spiral insert configuration is detailed in Figure 3.1.4. There was no measurable improvement in evaporator conductance.

In Phases 6 through 10, a 2.54 cm I.D. heat pipe was used with an evaporator that was coated with the Linde High Flux porous boiling surface. Phase 6 tests were performed with an open core (that is, no separator plate or condensate return tube) to establish a performance baseline.

Phase 7 and Phase 8 tests were performed using a 0.9 cm I.D. condensate return tube and a full-length separator plate oriented horizontally and vertically in Phases 7 and 8, respectively. No significant difference in axial transport capacity was found at low tilts; the orientation of the separator plate was of secondary importance.

In Phase 9 tests, the 0.9 cm I.D. condensate return tube was perforated periodically in the evaporator zone to allow liquid to bleed onto the evaporator surface in a roughly uniform fashion. This should result in a capacity increase since all of the condensate does not have to travel to the far end of the evaporator, resulting in a reduction in liquid pressure drop. A capacity increase of up to 60% was observed at low tilt angles.

In Phase 10, a plain tube of 1.2 cm I.D. was used as the condensate return. The transport capacity of this heat pipe was very close to the capability of the Phase 9 heat pipe. The Phase 10 heat pipe is close to having an optimum ratio of condensate tube diameter to heat pipe diameter. In vertical reflux operation, the Phase 10 heat pipe demonstrated a transport capacity that is a factor of 9 greater than possible with an open cross-section heat pipe, while at a tilt angle of 10°, a performance increase of 2.3 times was obtained.

In the following text and figures, the more significant test sequences will be discussed.

Detailed Discussions

Experimental values for burnout power, or critical heat flux, versus tilt angle are plotted in Figures 3.2.4 and 3.2.5 for R-11 and benzene in the Phase 10 heat pipes. Also shown on these plots are the predicted results based on the Section 2.2 modeling. The results are in excellent agreement considering the difficulty of measuring the exact value of burnout power. In Figure 3.2.5, two of the data points are indicated with "up" arrows. The data point at an 80° tilt was limited by the open pumped water loop temperature approaching 100°C, while the point at a 90° vertical orientation is the lower limit heat flux obtained during the oscillations discussed subsequently. The three "up" arrows shown in Figure 3.2.4 were caused by limitations in the power available for heating the evaporator.

In Figure 3.2.6, all burnout data for benzene and R-11 that was taken with the Phase 3, 4, 7, and 10 separators is compared as a function of tilt angle with the theoretical predictions. The experimental data are predicted to within ±25%. This level of agreement is quite satisfactory considering the accuracy limitation of the Lockhart-Martinelli and Owens models of two-phase pressure drop, and the uncertainty in identifying burnout heat flux. Exit and entrance qualities for the evaporator and condenser were set at 0.9 and 0.67, respectively, for all model calculations.

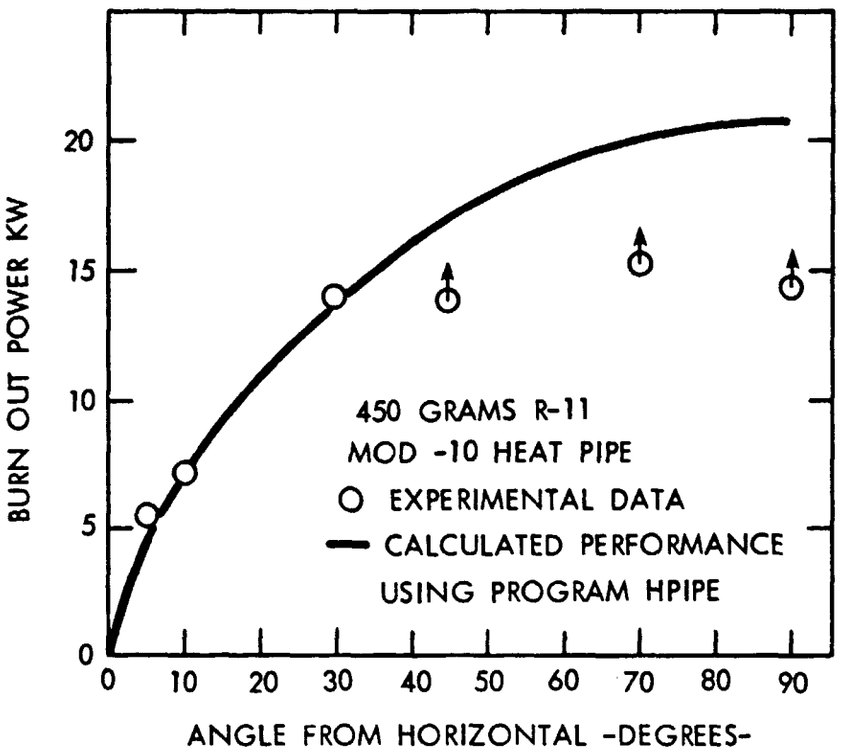

(3.2.4)

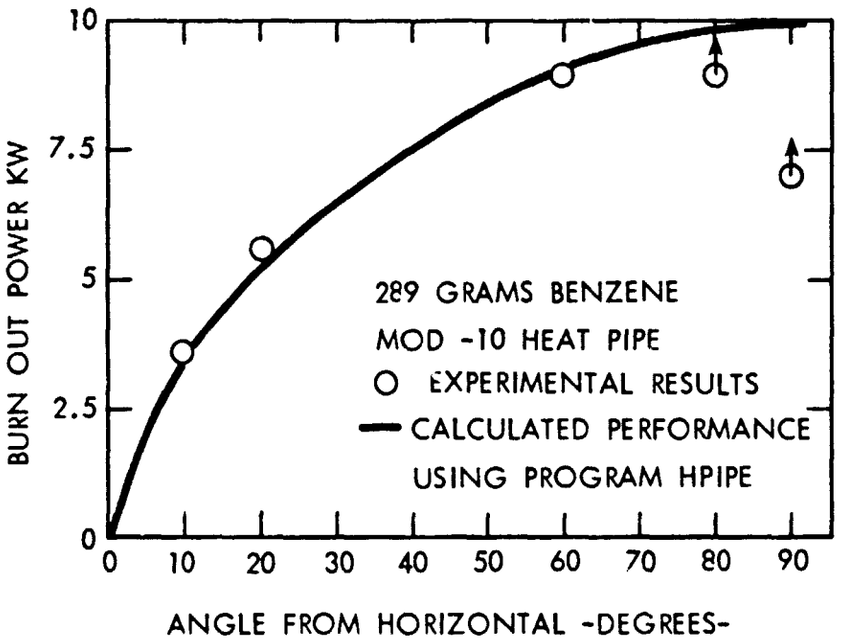

(3.2.5)

CRITICAL AXIAL HEAT FLUXES FOR PHASE 10 COCURRENT HEAT PIPE CHARGED WITH R-11 (FIGURE 3.2.4), AND WITH BENZENE (FIGURE 3.2.5).

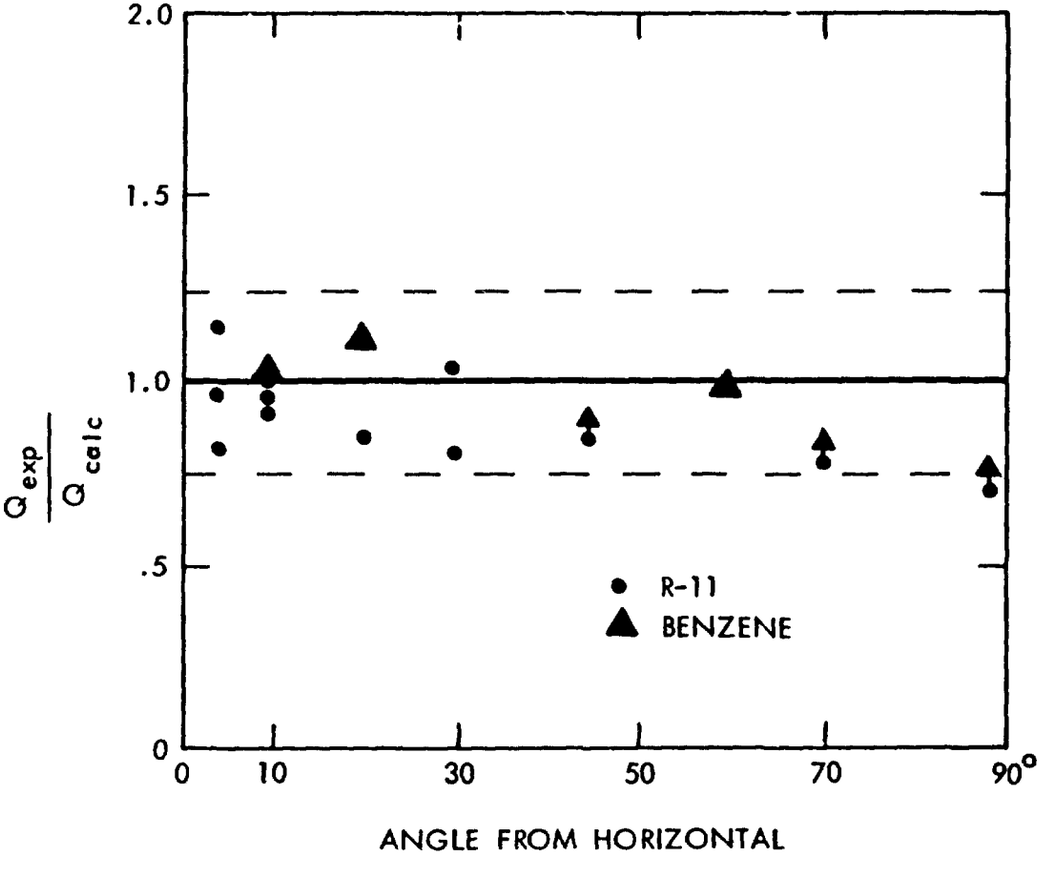

FIGURE 3.2.6. A COMPARISON OF EXPERIMENTAL CRITICAL HEAT FLUXES WITH CALCULATED VALUES FOR THE PHASE 3, 4, 7, AND 10 COCURRENT HEAT PIPES USING BENZENE AND R-11 WORKING FLUIDS.

When operated in a vertical or near-vertical orientation, the highest capacity evaporator system, Phase 10, tended to oscillate between two different modes of operation. This oscillation is shown in Figure 3.2.7, where the evaporator jacket temperature is plotted versus time. The period of the oscillation is approximately 24 minutes in this case. A check was made of the time constant associated with heating and cooling the entire heat pipe heating loop system and it was determined both experimentally and theoretically to be approximately 4 minutes. Thus, it appears that the observed oscillations were fundamental to the operation of the heat pipe and were not an artifact of the test setup.

The experimental data taken with Phase 10 indicate that the oscillations in heat pipe performance were due to changes in the thermal conductance of the condenser section. Bezrodny (17) has observed similar oscillations in the operation of bare tube thermosyphons. He attributes the oscillations to changes in the nature of the flow in the evaporator section. It was not possible in these tests to establish the cause of the oscillations in the Phase 10 heat pipe, and it is, therefore, not clear whether the qualitative observations of Bezrodny explain the changes noted here.

Figure 3.2.8 is a plot of overall conductance versus power for the 2.54 cm heat pipe using the Phase 10 separator. The working fluid is benzene. This graph, which is generally typical for all fluids, has several features of interest. First, it can be seen that the conductance versus power curves follow a nearly common curve until the burnout power for the particular angle is approached. The graph also shows that the burnout power is not sharply defined. Another interesting result is that the burnout power appears as a reduction in the conductance of the evaporator section of the heat pipe, a phenomenon also observed in the open core heat pipes of Section 3.2.1.

Figure 3.2.9 shows the evaporator and condenser conductances as a function of heat flux. Up to the point of burnout, both the evaporator and condenser conductances increase with heat flux. The peak evaporator conductances of 500 to 700 watts/°C obtained with the High Flux surface correspond to a heat

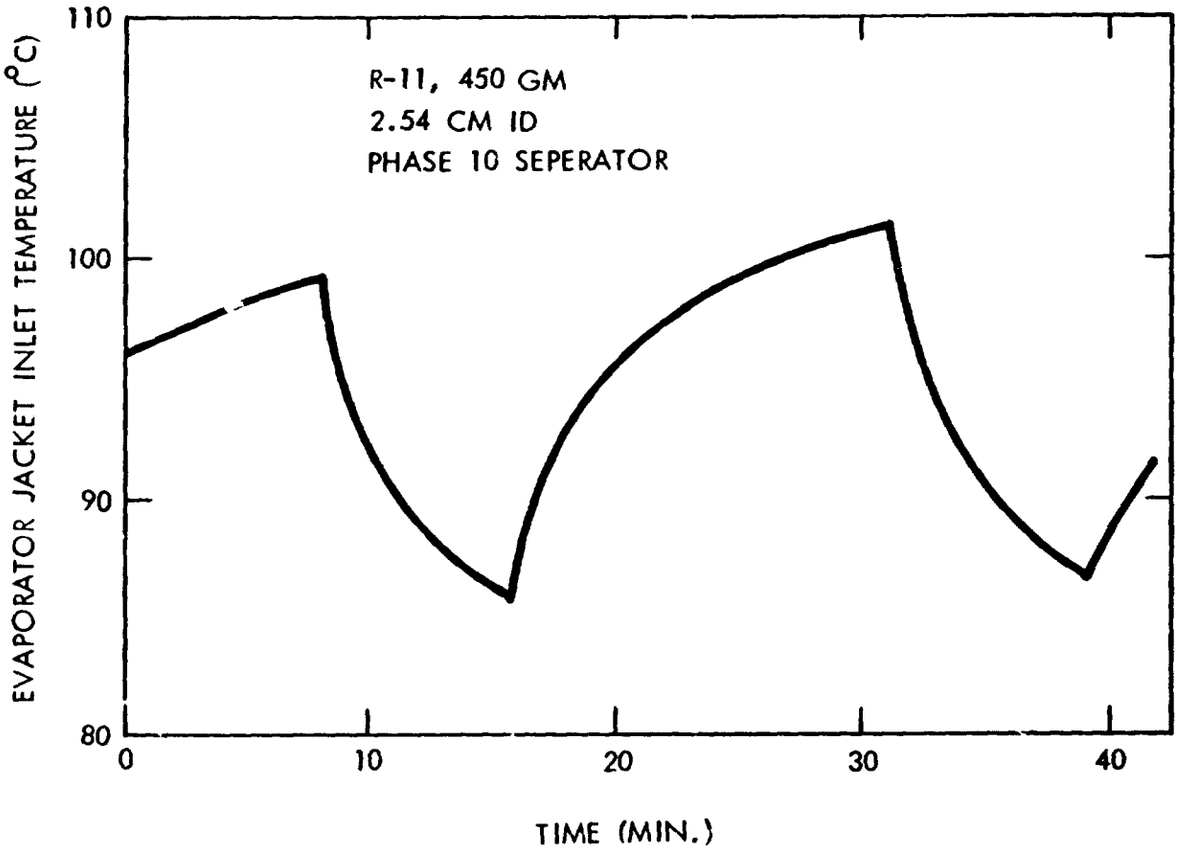

FIGURE 3.2.7. OSCILLATORY BEHAVIOR OF HEAT PIPE EVAPORATOR JACKET TEMPERATURE FOR THE PHASE 10 HEAT PIPE IN VERTICAL OPERATION WITH R-11 WORKING FLUID.

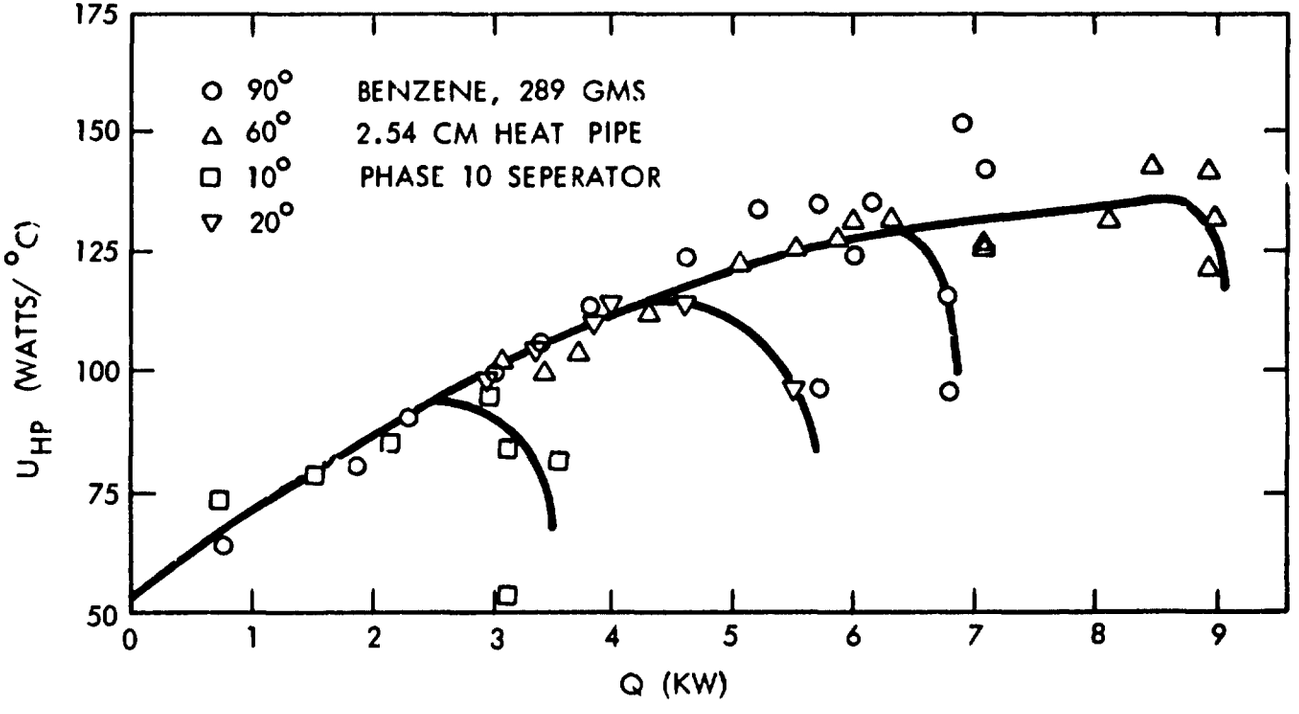

FIGURE 3.2.8. PHASE 10 COCURRENT HEAT PIPE CONDUCTANCE AS A FUNCTION OF TILT AND HEAT FLUX WITH BENZENE WORKING FLUID. TEMPERATURE RANGE = 40-80°C.

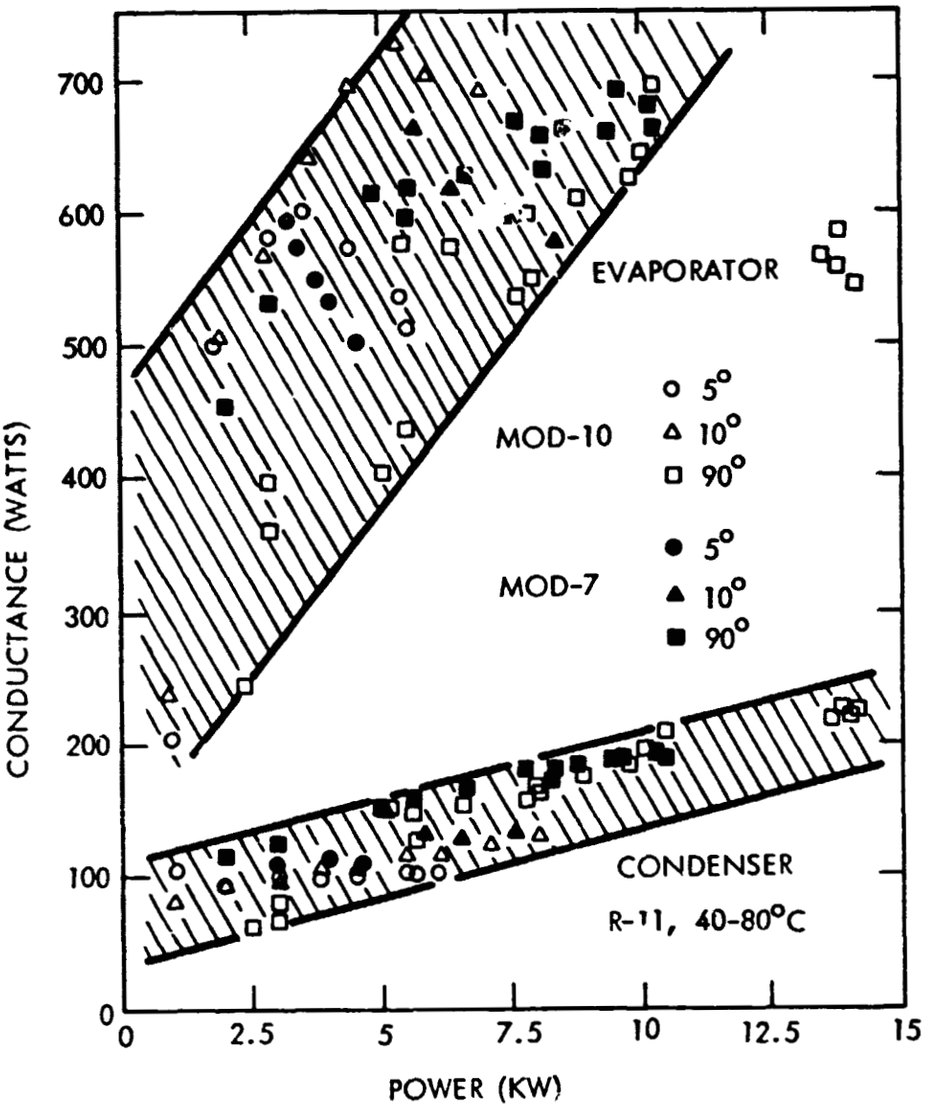

FIGURE 3.2.9. PHASE 10 HEAT PIPE CONDUCTANCE AS A FUNCTION OF TILT AND HEAT FLUX WITH R-11 WORKING FLUID.

transfer coefficient of 0.59 to 0.83 W/cm^2K (1040 to 1460 $Btu/hr\text{-}ft^2{}^\circ F$) over a radial heat flux density range of 3 to 18 W/cm^2 (9500 to 57,000 $Btu/hr\text{-}ft^2$). The condenser heat transfer coefficients fall in the range of 0.09-0.25 W/cm^2K for a radial heat flux density range of 2.70 to 16 W/cm^2K. It is clear that the condenser coefficient associated with the bare tube I.D. limits the overall heat pipe conductance, and is an area requiring further development.

4.0 SUMMARY AND CONCLUSIONS

By the introduction of a plate-and-tube separator assembly into a heat pipe vapor core, it has been demonstrated that axial transport capacity in reflux mode can be improved by up to a factor of 10. This improvement is largely the result of eliminating the countercurrent shear that commonly limits reflux heat pipe axial capacity. With benzene, axial heat fluxes up to 1800 W/cm^2 were obtained in the temperature range 40 to 80°C, while heat flux densities up to 3000 W/cm^2 were obtained with R-11 over the temperature range 40 to 80°C. These very high axial capacities compare favorably with liquid metal limits; the sonic limit for liquid sodium, for example, is 3000 W/cm^2 at 675°C. Computational models developed for these cocurrent flow heat pipes agreed with experimental data within ±25%, and a computer program HPIPE was written to facilitate optimization and calculation of heat transport limits for diverse cocurrent flowheat pipe designs.

The high axial transport limits obtainable under cocurrent flow conditions can lead to substantial reductions in heat exchanger cost through a reduction in the number of heat pipes required. However, to gain full benefit of the increase in axial capacity, the radial heat transfer resistances associated with vaporization and condensation must not account for an appreciable fraction of the hot stream/cold stream temperature difference. For the developmental heat pipe tested in this program, the evaporator conductance was improved through use of the Linde Highflux porous boiling surface, while no condenser improvement was attempted beyond the smooth-walled tube used in these tests. Heat transfer coefficients for the evaporator and condenser fell in the range 0.59-0.83 W/cm^2K and 0.09-0.25 W/cm^2K, respectively.

Using these heat transfer coefficients and radial heat flux densities in the 2 to 20 W/cm^2 range (as typical of many heat recovery applications), it can be seen that overall temperature losses for the evaporator and condenser could range from 2.5-34°C to 22-80°C, respectively. Since most heat recovery

applications have overall temperature differences of 250°C or less, it is clear that from 10% to one-third or more of the available temperature difference may be lost in the heat pipe. It is therefore clear that improvements in evaporating and condensing heat transfer coefficients will be needed in many cases to take full advantage of the cocurrent flow heat pipe's high flux capabilities.

These heat pipes are ideally suited for heat recovery applications with large hot stream/cold stream temperature differences and where radial and axial heat fluxes are sizable, as for example in stack gas recuperators and heat recovery boilers, or where relatively long heat pipes are required or indicated on the basis of performance and cost studies.

5.0 REFERENCES

1. F. W. Gay, Heat Transfer Means, U.S. Patent 1,725,906, U.S. Patent Office, Washington, D.C., August 27, 1929.

2. F. W. Gay, Cooling System for Underground Electric Transmission Lines, U.S. Patent 1,754,314, U.S. Patent Office, Washington, D.C., April 15, 1930.

3. E. L. Long, Means for Maintaining Permafrost Foundations, U.S. Patent 3,217,791, U.S. Patent Office, Washington, D.C., November 16, 1965.

4. E. D. Waters, U.S. Patents 3,763,931; 3,788,389; 3,828,845; 3,840,068; 3,902,547; and 3,935,900. Issued over period October 1973 to February 1976.

5. J. M. O'Byrne, Thermal Pile Analysis and Design, AIAA Paper No. 74-744, ASME Paper No. 74-HT-51, AIAA/ASME 1974 Thermophysics and Heat Transfer Conference, Boston, Massachusetts, July 15-17, 1974.

6. P. Dunn and D. Reay, Heat Pipes, Pergamon Press, Oxford, England, 1978. Reference to U.S. Patent 2,279,548 dated June 11, 1938.

6a. Gaugler, Patent No. 2,350,347, issued June 1944.

7. Y. Lee and V. Mital, "A Two-Phase Closed Thermosyphon," Int. J. of H. M. Transf., Vol. 15, p. 1695, Pergamon Press, 1972.

8. R. A. Ares, Cold-Heat Recovery for Air Conditioning, U.S. Patent 3,640,090, U.S. Patent Office, Washington, D.C., February 8, 1972.

9. J. E. Runyan and G. M. Grover, Heat Pipe and Method and Apparatus for Fabricating Same, U.S. Patent 3,753,364, U.S. Patent Office, Washington, D.C., August 21, 1973.

10. H. G. Barkmann, Heat Exchange System, U.S. Patent 3,788,388, U.S. Patent Office, Washington, D.C., January 29, 1974.

11. R. L. Pessolano, and R. B. Rhodes, Air-O-Space Heater Means for Recovering Heat From a Fluid Steam, U.S. Patent 3,884,292, U.S. Patent Office, Washington, D.C., May 20, 1975.

12. M. A. Ruch and G. M. Grover, Heat Pipe Thermal Recovery Unit Applications, 2nd International Heat Pipe Conference, Bologna, Italy, March 31-April 2, 1976.

13. G. B. Wallis, One-Dimensional Two-Phase Flow, McGraw-Hill, 1969.

14. G. B. Wallis and S. Makkenchery, J. Fl. Eng., Vol. 96, Ser. 1, No. 3, p. 297, 1974.

15. R. K. Sakhuja, Flooding Constraint in Wickless Heat Pipes, ASME Winter Annual Meeting, Detroit, Michigan, November 11-15, 1973. ASME Paper 73-WA/HT-7.

16. C. L. Tien and K. S. Chung, Entrainment Limits in Heat Pipes, 3rd International Heat Pipe Conference, Palo Alto, CA., May 22-24, 1978.

17. M. K. Bezrodny and A. Beloivan, High Temperature, Translated from Inzhenerno-Fizicheskii Zhurnal, Vol. 30, No. 4, p. 590, 1976. Copyright Plenum Publ. Corp., 227 W. 17th, N.Y., N.Y.

18. M. K. Bezrodny and A. A. Sakhatsh, Teploenergetika, Vol. 24, no. 3, p. 75, 1977.

19. H. Kusuda and H. Imura, "Stability of a Liquid Film in a Counter-Current Annular Two-Phase Flow," Bulletin of the JSME, Vol. 17, No. 114, December 1974.

19a. Z. Gorbis and G. Savchenkov, 2nd Int. Heat Pipe Conf., Bologna, Italy, March 31-April 2, 1976.

20. A. Abhat and H. Nguyenchi, 2nd International Heat Pipe Conference, Bologna, Italy, March 31-April 2, 1976.

21. H. Nguyen Chi and A. Abhat, 3rd International Heat Pipe Conference, Palo Alto, CA., May 22-24, 1978.

22. H. Nguyen Chi, M. Groll and Th. Dang-Van, AIAA 14th Thermophysics Conference, Orlando, Florida, June 4-6, 1979.

23. H. Nguyen Chi and M. Groll, AIAA 14th Thermophysics Conference, Orlando, Florida, June 4-6, 1979.

24. D. Briggs and E. Young, Fifth National Heat Transfer Conference, AICHE/ASME, Houston, Texas, August 5-8, 1962.

25. W. Kays and A. London, Compact Heat Exchangers, McGraw-Hill, New York, N.Y., 1964.

26. H. Mieth, Pet. M.E. and Press. Ves. and Piping Conference, Denver, Colorado, September 13-17, 1970. ASME Paper 70-P

27. R. Lockhart and R. Martinelli, Chem. Eng. Prog., 45 No. 1, p. 39.

28. W. Owens, Intl. Development in Heat Transfer, ASME, p. 363, 1961.

29. H. Schlicting, Boundary Layer Theory, McGraw-Hill, New York, N.Y., 1968.

30. R. Bird, W. Stewart, and E. Lightfoot, Transport Phenomena, John Wiley and Sons, Inc., N.Y., N.Y., 1960.

31. Flow of Fluids, Crane Technical Paper No. 410, Crane Co., N.Y., N.Y., 1976.

32. E. W. Saaski and P. C. Owzarski, Two-Phase Working Fluids for the Temperature Range 50 to 350°C, NAS3-20222, 1977.

33. J. Kemme, et al, Tenth Intersociety Energy Conversion Engineering Conference, Newark, Delaware, 1975.

34. G. M. Grover, Heat Pipe and Method and Apparatus for Fabricating Same, U. S. Patent 4,020,898, U. S. Patent Office, Washington, D.C., May 3, 1977.

APPENDIX A

COMPUTER PROGRAM "HPIPE"

PROGRAMMED IN

EXTENDED BASIC FOR THE PDP-11

```
20 DEFFN H(T)=233.147+.0208918*T-.669808E-3*T*T
30 DEFFN D0(T)=1.90521-.471017E-3*T-.324476E-5*T*T
40 DEFFN D2(T)=756.4*EXP(-2986.8/T)/T**.300665
50 DEFFN V0(T)=2.507E-4*EXP(840.172/T)
60 DEFFN V2(T)=-3.0672E-3+2.66248E-5*T-7.43805E-8*T*T+6.97587E-11*T**3
70 DEFFN F9(R)
71 IF R>2000 GO TO 74
72 FNF9=16/R
73 GO TO 75
74 FNF9=.219622/R**.43-.261297E-3*LOG(R)+5.95156E-3
75 FNEND
77 DEFFN Y9(X)
78 IF K8 < 2000 GO TO 81
79 FNY9 = (1+X**.1808)**1.01705*(1+X**.25)**3.15712
80 GO TO 82
81 FNY9 = (1+1.125*X**.75)**.218215*(1+X**.25)**3.31326
82 FNEND
90 DEFFN P(T)=4.4308E12*EXP(-3312.79/T)/T**.727083
100 DEFFN P9(Z,U1,U2)=-(R1*(Z*S3*(1-A/B)/(U2-U1)-A*C)+A*Z*S3)/B
110 READ Z0  !CONDENSATE RETURN TUBE LENGTH
111 DATA 99.7
120 READ A0,P0 !RETURN TUBE C.S. AREA AND WETTED PERIM.
121 DATA 1.119,3.75
130 READ Z1  !EVAPORATOR LENGTH
131 DATA 103.2
140 READ A1,P1 !EVAP. C.S. AREA AND WETTED PERIM.
141 DATA 4.107,12.21
150 READ Z2  !ADIABATIC LENGTH
151 DATA 14.0
160 READ A2,P2 !ADIA. C.S. AREA AND WETTED PERIM.
161 DATA 4.107,12.21
170 READ Z3  !CONDENSER LENGTH
171 DATA 115.6
180 READ A3,P3 !COND. C.S. AREA AND WETTED PERIM.
181 DATA 5.065,7.98
190 READ Z4  !SEPARATOR LENGTH IN ADIA.
191 DATA 14
200 READ A4,P4  !SEP. C.S. AREA AND WETTED PERIM. IN ADIA. ZONE
201 DATA 2.405,6.43
205 READ Z5  !SEPARATOR LENGTH IN COND.
206 DATA 94.6
210 READ A5,P5  !C.S. AREA AND PERIM. ON EACH SIDE OF SEP. IN COND. ZONE
211 DATA 2.405,6.43
215 READ X0,X1  !EVAP. INLET AND OUTLET QUALITY
216 DATA 0,.999
220 READ X2,X5  !COND. INLET AND OUTLET QUALITY
221 DATA .5,0
230 READ T2  !INITIAL SATD. VAP. TEMP.
231 DATA 80
240 READ H1,H2  !MIN. AND MAX. HEAT FLUXES (W)
241 DATA 100,25000
250 READ H0  !AVAIL. LIQUID HEAD WHEN OPERATED VERTICALLY
```

```
251 DATA 99.7
260 READ A8  !TILT ANGLE W.R.T. HORIZ., DEGREES
261 DATA 90
300 READ G  !GRAV. ACC.
301 DATA 980.6
310 A9=SIN(.0174533*A8)
320 Z9=H0*A9  !AVAILABLE HEAD
330 T=T2+273.15:U7=.001:H9=FNH(T)
340 L1=H1/H9:L2=H2/H9
349 PRINT
350 PRINT"  Q(W)          MASS FLOW     PRESS. HEAD       TILT          TEMP."
351 PRINT"DP-EVAP         DP-ADIA.      DP-SEP/ADIA     DP-TUBE        DP-COND"
352 PRINT"---------       ---------     -----------     --------       -------"
410 Y0=FNV0(T):Y2=FNV2(T):W0=FND0(T):W2=FND2(T)
415 A=W0/W2-1:H1=W0*G*Z1*A9/(X1-X0)
420 F0=.5*Z5/Z3:X3=X2+F0*(X5-X2):X4=X5-(X3-X2):F2=W2*(1/X1-1)**2/W0
430 X6=1+A*X2:X7=1+A*X4:X8=1-X1:X9=1+A*X1
440 C0=4/(P0*Y0):C1=4/(P1*Y0):C2=4/(P2*Y2):C3=4/(P5*Y0):C4=4/(P4*Y2)
450 C5=4/(P2*Y0):C6=4/(P4*Y0):C7=4/(P5*Y2):C8=4/(P1*Y2)
460 B0=.5*P0*Z0/(W0*A0**3):B1=.5*P1/(W0*A1**3):B2=.5*P2/(W2*A2**3)
470 B3=.5*P5/(W2*A5**3):B4=.5*P4*Z4/(W2*A4**3):B5=B1*(W0/W2)
474 E4=X9/(2*W0*A4*A4):E5=E4*(A4/A5)**2
475 IF Z2<.01 GO TO 495
476 Z6=Z2-Z4
477 IF Z4<.01 GO TO 490
478 IF ABS(Z4-Z2)<.01 GO TO 485
480 E2=E4:B=A4/A2:GO TO 500
485 E2=E4:B=A4/A1:GO TO 500
490 E2=E5:B=A5/A2:GO TO 500
495 E2=E5:B=A5/A1:Z6=0
500 E2=.45*(1-B)*E2:E3=30*(2+A*(X3+X4))/(W0*A5*A5) !ENTRANCE/EXIT FACTORS
510 G1=-1/(W2*FNP(T)*A1*A1):V1=1/(W0*A1*A1)
515 IF Z5<.01 GO TO 550
520 F5=W2*(1/X2-1)**2/W0:F6=W2*(1/X4-1)**2/W0
525 G5=G1*(A1/A5)**2:V5=1/(W0*A5*A5)
530 H5=W0*G*Z5*A9/(X3-X2):H6=H5*(X3-X2)/(X5-X4)
540 O5=LOG((1+A*X2)/(1+A*X3)):O6=LOG((1+A*X4)/(1+A*X5))
550 O1=LOG((1+A*X0)/(1+A*X1))
560 B=A0/A5:E0=.225*(1-B)/(W0*A0*A0):E1=.45*B**3/(1+B)
570 E1=(E1+1/(1+B)**2)/(2*W0*A0*A0):E6=60*B*B/(W0*A0*A0*(1+B)**2)
590 U6=-1:U9=1E-12
600 M=(L1+L2)/2:M4=(L2-L1)/4
610 FOR I=1 TO 100
615 M0=M*X8:M1=M*X1:M2=M*M:M6=F0*M1:M8=M1*M1
700!CONDENSATE TUBE PRESSURE DROP- FRICT. AND ENTR.
710 F=FNF9(C0*M)
720 S0=B0*M2*F:S1=(E0+E6*FNF9(4*M/(Y0*(P1-P0))))+E1)*M2
800!ADIABATIC ZONE
805 IF Z2<.01 GO TO 895
810 F=FNF9(C2*M1):X=F2*FNF9(C5*M0)/F:K8=C5*M0:Y=FNY9(X)
820 S3=Y*B2*M8*F
830 S5=S3*Z6:GO TO 900
895 S5=0
```

```
900!EVAPORATOR ZONE
905 F=FNF9(C8*M1):X=F2*FNF9(C1*M0)/F:K8=C1*M0:Y=FNY9(X)
910 B=G1*M2:C=V1*M2:B6=1+B*X0:B7=1+B*X1
911 IF B6<0 GO TO 1290:IF B7<0 GO TO 1290
915 R1=LOG(B7/B6)
920 S3=-Y*B5*M8*F/X9  !INLET DP/DZ COMPAT. WITH EXIT DP/DZ
930 S4=FNP9(Z1,X0,X1)
940 S2=H1*(Q1+R1)/(B-A)  !GRAV. DP
1000!SEPARATOR-ADIA. SECTION
1004 S7=E2*M2  !ENTRANCE
1005 IF Z4<.01 GO TO 1095
1010 F=FNF9(C4*M1):X=F2*FNF9(C6*M0)/F:K8=C6*M0:Y=FNY9(X)
1030 S6=Y*B4*M8*F  !FRICT. DP
1090 GO TO 1100
1095 S6=0
1100!CONDENSER ZONE
1105 IF Z5<.01 GO TO 1195
1110 M3=M1/X2:M5=M3*(1-X2):M2=M3*M3
1111 R4=E3*M2*FNF9(C3*M3)  !EXIT/ENTRANCE AT PLATE TERMINATION
1115 B=G5*M2:C=V5*M2:B6=1+B*X2:B7=1+B*X3:B8=1+B*X4:B9=1+B*X5
1116 IF B6<0 GO TO 1290:IF B7<0 GO TO 1290
1117 IF B8<0 GO TO 1290:IF B9<0 GO TO 1290
1118 R1=LOG(B7/B6)
1120 F=FNF9(C7*M1):X=F5*FNF9(C3*M5)/F:K8=C3*M5:Y=FNY9(X)
1125 S3=-Y*B3*M8*F/X6:R5=FNP9(Z5,X2,X3)
1130 R6=H5*(R1+Q5)/(B-A)  !GRAV. DP
1150 M5=M3*(1-X4):R1=LOG(B9/B8)
1160 F=FNF9(C7*X4*M3):X=F6*FNF9(C3*M5):Y=FNY9(X)
1165 S3=-Y*B3*(M3*X4)**2*F/X7:R7=FNP9(Z5,X4,X5)  !FRICT.+ ACC. DP
1170 R8=-H6*(Q6+R1)/(B-A)  !GRAV. DP
1190 GO TO 1200
1195 R5=0:R6=0:R7=0:R8=0
1200!PRESSURE BALANCE
1210 S8=W0*G*Z2*A9/X9  !GRAV DP IN ADIA.
1220 S9=W0*G*Z9
1230 S=S9-S8-S7-S6-S5-S4-S2-S1-S0
1240 S=S-R4-R5-R6-R7-R8
1250 IF S<0 GO TO 1290
1260 M=M+M4:U8=ABS(M/U9)-1
1270 IF ABS(U8)<U7 GO TO 2000
1280 U9=M:GO TO 1300
1290 M=M-M4:U6=1
1300 M4=M4/2:NEXT I
2000!PRINT STATEMENTS
2001 IF U9<1.10E-12 GO TO 3000
2002 IF U6<0 GO TO 3010
2010 Q=M1*H9  !LATENT HEAT TRANSFER
2020 PRINT Q,M,S9,A8,T2
2025 U1=S2+S4:U2=S5:U3=S6+S7:U4=S0+S1:U5=R4+R5+R6+R7+R8
2030 PRINT U1,U2,U3,U4,U5
2050 PRINT
2099 GO TO 9999
3000 PRINT"MASS FLOW LESS THAN MIN. VALUE":GO TO 9999
3010 PRINT"MASS FLOW EXCEEDS MAX. VALUE"
```